

SLOVAK UNIVERSITY OF TECHNOLOGY IN BRATISLAVA
Faculty of Electrical Engineering and Information Technology

Ing. Vendula Vrtalová

Dissertation outline

Development and implementation of measurement of dosimetric quantities using latent trace detectors

Reg. No.: FEI-104396-119279

**to obtain the academic title philosophiae doctor, abbreviated as PhD.,
in the doctoral study program Nuclear Power Engineering,
in the field of Electrical and Electronics Engineering**

Bratislava, 2026

The dissertation thesis was prepared as part of a full-time doctoral study program at the Institute of Nuclear and Physical Engineering, Faculty of Electrical Engineering and Information Technology, Slovak University of Technology in Bratislava.

Submitted by: **Ing. Vendula Vrtalová**
Institute of Nuclear and Physical Engineering, FEI STU in Bratislava,
Ilkovičova 3, 841 04, Bratislava

Supervisor: **doc. Ing. Branislav Vrban, PhD.**
Institute of Nuclear and Physical Engineering, FEI STU in Bratislava,
Ilkovičova 3, 841 04, Bratislava

Opponents: **doc. Ing. Milan Štefánik, Ph.D.**
Department of Nuclear Reactors, FNSPE CTU in Prague,
V Holešovičkách 2, Prague 8, 180 00, Czechia

doc. RNDr. Monika Müllerová, PhD.
Department of Nuclear Physics and Biophysics, FMFI UK,
Mlynská dolina F-1, 842 48 Bratislava

The outline was sent on 23th of January, 2026

The defense of the dissertation thesis is taking place on 26th of February, 2026, at 10:00, at the Faculty of Electrical Engineering and Information Technology STU in Bratislava, Ilkovičova 3, 841 04 Bratislava.

Prof. Ing. Vladimír Kutiš, PhD.
Dean of the Faculty
Faculty of Electrical Engineering and Information Technology
Slovak University of Technology in Bratislava

Abstract

The dissertation thesis aimed to develop the methodology for the use of the solid-state nuclear track detectors (SSNTD) made of poly-allyl diglycol carbonate (PADC) in the detection of ionizing radiation, and to use the proposed methods in applications. The thesis focused mainly on fast neutron detection, however, experiments on the ion detection were also performed.

The state-of-art brings the research performed within the thesis into the context of the current trends in SSNTDs applications. The methods introduced within the thesis were based on the theoretical background summarized in the Thesis for the dissertation exam of the author of the thesis, and on the experience based on a number of experiments performed by the author of the thesis. The author has also developed several codes for the analysis of the detectors. The results are presented in the form of the individual experiments, where some of the experiments were designed to verify the properties of PADC detectors under specific conditions, and the other experiments were proposed to verify the developed methodology in practice. The directions for the continuation of the research were proposed, based on the findings presented.

Abstrakt

Cílem disertační práce bylo vyvinout metodiku pro použití detektorů stop v pevné fázi (SSNTD, z angl. *solid-state nuclear track detectors*) vyrobených z polyallyl diglykol karbonátu (PADC, z angl. poly-allyl diglycol carbonate) při detekci ionizujícího záření a aplikovat navrhované metody v praktických úlohách. Práce se zaměřila především na detekci rychlých neutronů, byly však provedeny i experimenty zaměřené na detekci iontů.

Současný stav problematiky uvádí výzkum realizovaný v rámci dizertační práce do kontextu současných trendů v aplikacích SSNTD. Metody představené v dizertační práci vycházely z teoretického základu shrnutého v písemné práci k dizertační zkoušce autorky dizertační práce a ze zkušeností získaných na základě řady experimentů provedených autorkou dizertační práce. Autorka také vyvinula několik kódů pro analýzu detektorů. Výsledky jsou prezentovány ve formě jednotlivých experimentů, přičemž některé z experimentů byly navrženy tak, aby ověřily vlastnosti detektorů PADC za daných podmínek, jiné experimenty byly navrženy tak, aby ověřily vyvinutou metodiku v podmínkách reálného použití. Na základě předložených zjištění byly navrženy směry pro pokračování výzkumu.

Contents

Abstract	3
Abstrakt	3
List of abbreviations and symbols	5
Introduction.....	7
1. Overview of the current state	8
2. Objectives of the dissertation.....	9
3. Methodology	10
3.1. SSNTDs materials	10
3.2. Formation of a latent track	10
3.3. Neutron detection	11
3.4. Background components	11
3.5. Installation during the experiment	12
3.6. Etching.....	12
3.7. Evaluation	15
3.8. Codes developed at STU	16
3.9. Other programs.....	17
4. Results.....	18
4.1. Acceptance testing with Pu-Be neutron source	18
4.2. Etching Time Effects on Fast Neutron Response in PADC Detectors.....	21
4.3. Combination of PADC and radiator for neutron radiography.....	24
4.4. PADC fading study.....	25
4.5. First demonstration of neutron imaging using PADC	26
4.6. D-D neutron spatial distribution measurement	27
5. Conclusion	29
Závěr	30
References.....	31
Publications of the author related to the thesis	35
Citations of the publications of the author of the thesis	37

List of abbreviations and symbols

BDD	Boron-doped diamond	
EURADOS	European Radiation Dosimetry Group	
FAINE	Fast Artificial Intelligence Neutron Detection System	
HDPE	High-density polyethylene	
LET	Linear Energy Transfer	
MCNP	Monte Carlo N-Particle Transport Code System	
NARP	National Action Radon Plan	
PADC	Poly-allyl Diglycol Carbonate	
REL	Restricted Energy Loss	
SSNTD	Solid-State Nuclear Track Detector	
SRIM	Stopping and Range of Ions in Matter	
STU	Slovak University of Technology in Bratislava	
SW4A: PADC	Software for Analysis of Ionizing Radiation Measurement Data from PADC	
WG	Working group	
A	Mass number	(-)
A_d	Size of the etched area of the detector	(m ²)
A_f, C_f	Function parameters	(1/eV)
A_1	Ratio of the real event area to the area of the interpolated ellipse	(-)
AREA	Real event area	(m ²)
B_f, D_f	Function parameters	(-)
CONV	Convexity along the main axis of the event	(-)
D	Diameter of the etched track from the fission fragment	(m)
c	Speed of light in vacuum	(m/s)
d_1, d_2	Thickness of the detector before and after etching	(m)
E	Energy	(eV)
dE/dx	Mean energy loss	(eV/m)
FOCUS	Event focus level	(-)
GREY	Gray value averaged over the entire event area	(-)
h	Thickness of the etched layer	(μm)
$H^*(10), H_r^*(10)$	Ambient dose equivalent	(Sv)
I	Excitation potential of a given substance	(eV)
k	Direction of the fit	(-)
K	Constant in the Bethe-Bloch equation	(eV·m ² /mol)
L	Particle path length in the detector	(m)
m_1, m_2	Mass of the detector before and after etching	(kg)
m_e	Electron mass	(kg)
MIN	Minor axis of the ellipse	(m)
N_A	Avogadro's constant	(1/mol)
r_e	Electron radius	(m)
R	Particle range in a substance	(m)
R^2	Coefficient of determination	(-)
SHARP	Event edge sharpness	(-)
SYMM	Symmetry along the main axis of the event	(-)
t	Etching time	(s)

v	Particle velocity	(m/s)
V	Etching ratio, or sensitivity	(-)
V_b	Bulk etch rate	(m/s)
V_t	Track etch rate	(m/s)
W_{max}	Maximum energy loss per collision	(eV)
x, y	Coordinates	(m)
XT/MJ	Projected length of the track/Major axis of the ellipse	(m)
z	Proton number of the incident particle	(-)
Z	Proton number of a given substance	(-)
β	Factor expressing the ratio of v and c	(-)
γ	Lorenz factor	(-)
δ	Angle between the wall of track and trajectory of the inc. particle	(rad)
δ_c	Critical angle	(rad)
ρ	Density	(kg/m ³)
μ	Mean value	(-)
μ_f, σ_f	Function parameters	(eV)
σ	Standard deviation	(-)

Introduction

Since ionizing radiation is inextricably linked to human existence, whether in the form of natural radiation or radiation from artificial sources, research into methods for its accurate detection is constantly evolving. The nature of a particular application determines the required properties of the detector. Requirements often focus on the nature of the detector's function – whether the application requires a real time response (closely linked to the need of an electrical signal transmission) or whether it relies on signal integration. Another important aspect is the ability to distinguish between detected particles in mixed fields, such as (n, gamma) fields. Other parameters to consider when selecting a detector include its size, durability, and cost.

The field of solid-state nuclear track detectors (SSNTD) has been studied since the 1950s, when Young observed the fission fragments in lithium fluoride film. Subsequent etching with hydrofluoric acid and glacial acetic acid led to the creation of etched tracks of a pyramid shape. Following this demonstration of the enlargement of latent tracks, the formation of which was already known from detectors such as cloud chambers and bubble chambers, a wide range of materials became the subject of research. It was found that the ability to form latent tracks correlates with the low conductivity of the detection material – crystals, glass, and plastics proved to be suitable for use as SSNTDs.

Passive SSNTDs are also suitable for long-term measurements and are sensitive to heavy charged particles; electrons and photons do not create latent tracks. They can be manufactured in various shapes and sizes, and the cost of the detectors is low compared to other detection techniques.

Since the relationship between the measured dose and the density of etched tracks is linear, the analysis of detectors from a dosimetric point of view is often based on counting etched tracks areal density. Performing such analysis manually is a time-consuming process that might be problematic for routine dosimetric measurements. With the development of automation and computing technologies that enable automated detector analysis, SSNTDs have gained popularity.

The aim of the dissertation thesis is to familiarize readers with the methodology developed for the use of plastic SSNTDs made of polyallyl diglycol carbonate (PADC) in particle detection. The thesis, the same as this text, is divided into four main chapters: State of the Art, Methodology, Results, and Conclusion.

The chapter State of the Art puts the research conducted at the Slovak University of Technology in Bratislava (STU) in the context of current global research and provides an overview of the possible applications of SSNTDs.

Methodology contains a summary of methods, tools, and findings that have been identified as relevant for individual applications of PADC detectors, based on the theory introduced in the Thesis for the dissertation exam of the author of this work. The chapter describes individual aspects related to the use of PADC, codes developed at STU for the analysis of measurement results, and software tools used in the experiment design phase.

The chapter Results discusses individual experiments carried out at STU as part of the doctoral studies of the author of this work. In the thesis, the chapter is divided into three parts, the first of which presents work carried out to understand the properties of PADC detectors under various conditions. The second part provides an introduction to experiments in which PADC detectors were used in specific applications. The last part describes experiments currently underway at STU. This work describes the selected experiments.

The conclusion summarizes the presented findings and identifies their contribution to the individual topics of the dissertation, as defined in the dissertation thesis. It also identifies potential directions for future research in the field of SSNTDs.

1. Overview of the current state

SSNTDs are currently used in a wide range of applications, some of which are presented below.

A team of authors from India developed the autoTRAK_n analysis program [1] for neutron spectrometry. In the first experiments, the program was verified in the detection of neutrons from three sources with different spectra (^{252}Cf , Am-Be, and D-T). The etched tracks were analyzed in the autoTRAK_n program, which can measure several parameters such as diameter, major axis, minor axis, depth, etc. From this data, the range of the particles in the detector was calculated and compared with the results of the SRIM code [2], which led to obtaining information about the original incident particle energy. The program can also evaluate the ambient dose equivalent $H^*(10)$.

The European Radiation Dosimetry Group (EURADOS), a network of European institutions, companies, and scientists, has been registered since 2001. It consists of several working groups (WGs), focused on various areas of dosimetry. WG2 aims to harmonize individual monitoring and is divided into individual task groups. One task group focuses on improving the quality of PADC material for neutron dosimetry. The group's work began with a review of state-of-the-art practices in PADC dosimetry and the identification of key topics requiring further research [3]. The review was followed by experiments with PADC material from different suppliers, which were processed at several European institutions. The goal is to work with manufacturers to improve the quality of detector material, thereby minimizing uncertainty caused by the internal background signal. Two representatives of STU, V. Vrtalová and B. Vrban, joined this task group in 2022, and V. Vrtalová became the head of the task group focused on PADC detectors at the beginning of 2025.

With advances in artificial intelligence, attempts have been made in recent years to implement deep learning and neural networks in the evaluation of signals from PADC. The paper [4] describes the development of the Fast Artificial Intelligence Neutron Detection System (FAINE) for analysis based on PADC detectors and deep learning. PADC detectors irradiated with neutrons were etched and scanned. Events corresponding to neutron tracks were manually selected, and 80 % of the images were used to train a U-Net convolutional artificial neural network. The accuracy of the system was tested on the remaining 20 % of the data set, where an accuracy of 96.7 % was achieved.

The emission of α particles from animal bone samples was measured in [5]. The bones were burned, and the ashes were placed at the bottom of a 12 cm high beaker. In the first run of the experiment, the PADC detector was placed directly on the bone ashes, and in the second run, the detector was placed at a distance of 2 cm. The detectors were left in the beaker for 60 days to achieve radioactive equilibrium. Several detectors were calibrated using ^{241}Am . The emission of α particles was determined based on the density of etched tracks. The results were compared with previous studies. The results of the detectors at both distances were also compared, and a method for identifying radionuclides was proposed based on the distance of the detector from the sample under investigation.

The issue of radon is very topical, with many countries working on their national radon action plans (NARP). Research in [6] focused on measuring radon in various building materials from the Jazan region of Saudi Arabia. More than 100 samples of building materials (marble, granite, brick, ceramics, sand, gypsum) were collected, dried, and placed at the bottom of special irradiation chambers with a PADC detector. The density of α particle tracks enabled determination of the radon concentration, radon activity, α index, effective dose, and uranium concentration. The research showed that of all the materials tested, granite had the highest concentration of radon activity (an average of 505 Bq/m^3), while the internationally recognized limit is 600 Bq/m^3 . The article also puts its results in the context of other experiments from the Middle East. The same experimental approach was used in [7] to measure radon concentration in geopolymers and in [8] to determine radon concentration in food in the Jazan region.

2. Objectives of the dissertation

The following topics were identified for the dissertation thesis based on the results of the Thesis for the dissertation exam submitted by the author.

I. Topic: Experimental verification of the response of TASTRAK detectors to various types of radiation and the change of response due to the usage of radiators and degraders designed using SRIM.

II. Topic: Unification of the etching process, its comparison with the approaches of other laboratories, and the estimation of the correction factors in case of deviation from the recommended procedure.

III. Topic: Experimental verification of the effect of various conditions on the performance of TASTRAK detectors, such as ageing.

IV. Topic: Expansion of the Neutron CR-39 simulation code to be suitable for its usage in experiments, by changing the geometry of the simulated model and adding the possibility to simulate the neutron energy dependence of the number of etched tracks.

V. Topic: Establishment of the methodology of measurement using these detectors together with appropriate corrections.

3. Methodology

This chapter summarizes the important properties of PADC detectors, and the methods used in the experiments conducted as part of the thesis.

3.1. SSNTDs materials

Track detectors represent a group of passive detectors that include a wide range of materials such as minerals, glass, and plastics. Their common properties include their behavior in an electric field, where they belong to non-conductors or weak semiconductors, and their good light transmittance.

Currently, one of the most used materials is PADC polymer with a linear structure. The material has a high degree of homogeneity and suitable optical properties. From a chemical perspective, it consists of three constituents: hydrogen, oxygen, and carbon, with the chemical formula $C_{12}H_{18}O_7$. The TASTRAK PADC detectors manufactured by Tasl Ltd [9] were used in the experiments described in the thesis.

3.2. Formation of a latent track

The formation of a latent track as a result of the impact of a heavy charged particle can be divided into three parts: physical, physiochemical, and chemical [10].

The physical part takes place within $1E-15$ s after the particle incidence [10]. Generally, three principles apply when a particle interacts with matter: the electrostatic force between the impacting particle and the electron shell, which leads to excitation and ionization; the electrostatic force between the impacting particle and the nucleus, which leads to the displacement of the atom, and the emission of electromagnetic radiation (bremsstrahlung or Cherenkov radiation). The last principle is significant either in the field of relativistic energies or for light charged particles. In the case of ions, i.e., heavy charged particles, the energy loss of the incident particle is described by the first two principles. The average energy loss $-\frac{dE}{dx}$ (eV/m) is defined by the Bethe-Bloch equation, which (considering quantum mechanics) has the form

$$-\frac{dE}{dx} = KZ^2 \frac{Z}{A} \frac{\rho}{\beta^2} \left[\frac{1}{2} \ln \frac{2m_e \gamma^2 c^2 \beta^2 W_{max}}{I^2} - \beta^2 - \frac{\delta(\beta\gamma)}{2} \right], \quad (1)$$

where the constant K (eV·m²/mol) is expressed as $K = 4\pi N_A r_e^2 m_e c^2$, where N_A (1/mol) is Avogadro's constant, r_e (m) is the radius of an electron, m_e (kg) is the mass of an electron, c (m/s) is the speed of light in a vacuum, z (-) is the proton number of the incident particle, Z (-) is the proton number of the given substance, A (-) is the mass number of the substance, ρ (kg/m³) is its density, β (-) is a factor expressing the ratio of the velocity of the incident particle v (m/s) to the speed of light in a vacuum c ($\beta = \frac{v}{c}$), γ (-) is the Lorentz factor $\gamma = \sqrt{1 - \beta^2}$, W_{max} (eV) is the maximum energy loss in a single collision, and I (eV) is the excitation potential characteristic of the given substance. Equation 1 also includes a correction for electron shells $-\beta^2$ and a correction for the density effect $-\frac{\delta(\beta\gamma)}{2}$.

The dependence of energy loss on penetration depth is described by the Bragg curve, with the Bragg peak corresponding to increased energy losses at the end of the path of the incident particle. The amount of energy transferred to the detector material is expressed by linear energy transfer (LET).

From the perspective of the incident particle, the energy losses described above determine the range of the particle in the material R (m), described by the equation

$$R(E) = \int_E^0 \left(\frac{dE}{dx} \right)^{-1} dE. \quad (2)$$

Energy loss increases at the end of the particle's path, in accordance with the Bragg curve.

δ -rays are secondary electrons released from the atomic shells of a material because of the impact of a heavy charged particle. Some of these electrons can have high energy, which they transfer to the material at a large distance from the path of the original particle. Restricted energy loss (REL) is a quantity that considers the energy transferred in the vicinity of the path of the incident particle, based on the defined δ -ray energy limit. Various models [11] developed over the years, establish criteria for the formation of a latent track, often based on REL, considering δ -rays. However, none of the present models covers all the effects observable in the formation of a latent track.

The physical part is followed by the physiochemical part, between 1E-15 s and 1E-12 s [10]. During this phase, intermediate species are formed (free radicals, i.e., atoms, molecules, or ions with an unpaired valence electron, which makes them chemically reactive).

The final phase of latent track formation is the chemical part (occurring from 1E-12 s to 1E-6 s) [10], in which new chemical bonds are formed in the vicinity of the trajectory of the incident particle.

3.3. Neutron detection

Neutrons do not create latent traces directly; the conversion reactions are used for their detection. These can occur either directly in the detector material or in an additive layer of material, known as a radiator. In the case of fast neutron detection, the most commonly used method is the interaction of the neutron with a hydrogen nucleus, where elastic scattering occurs and the recoiled proton creates a latent track. Thanks to the large amount of hydrogen in the PADC polymer structure, fast neutrons can be detected directly using a PADC detector [12]. In addition to interactions with hydrogen nuclei, reactions with carbon and oxygen nuclei can also occur in the PADC material, which can lead to the production of α particles. These are threshold reactions with thresholds in the order of units of MeV. In the thesis, the high-density polyethylene (HDPE) or Kapton tape was used as a radiator.

Thermal neutron detection is possible due to the addition of a radiator containing a material such as boron, where the (n, α) reaction occurs [13]. The thesis demonstrated the use of boron-doped diamond layers (BDD) as a radiator for thermal neutron detection.

In some experiments, it is desirable to shield part of the incident radiation (for example, in the mixed field where multiple kinds of particles could be detected). In such cases, it is advisable to use a suitable degrader [14], i.e., a material that captures part of the incident radiation. In the thesis, an aluminum degrader was designed for an experiment in measuring the spatial distribution of neutrons from a D-D fusion reaction.

3.4. Background components

The background signal registered by PADC detectors can have three components [15]:

- Natural background – tracks caused by the impact of cosmic radiation or due to the presence of radon and its daughter products,
- Scratches and dust – damage caused by improper handling, and
- Intrinsic background – bubbles and other shapes originating from the process of polymerization.

Various laboratories have defined tests to evaluate whether the ratio of the background signal is acceptable. Some of these tests have been verified in [16].

Since the handling of detectors between delivery and etching plays a significant role in signal processing, certain procedures have been introduced at STU. Detectors are stored in a freezer at a temperature of -18 °C. Polyethylene bags are used for transport to protect detectors from external effects. Plastic gloves must be worn when handling unetched detectors.

3.5. Installation during the experiment

3D-printed holders are used to fix PADCs during the experiment at STU, allowing for the simultaneous exposure of multiple detectors. The holders can be assembled into modules, such as the KOSTKA experimental device, which will be described in the Results chapter. During each experiment, it is necessary to consider potential environmental influences and, if necessary, include a suitable degrader.

Several types of diffusion chambers are used at STU to measure radon activity concentration. Some of the chambers used are supplied by Tasl Ltd., while others were designed at STU by Jakub Lüley.

3.6. Etching

In SSNTDs materials, the rate of material removal along the particle path (i.e., along the latent track), the track etch rate V_t (m/s) is greater than the rate of material removal from the detector surface, the bulk etch rate V_b (m/s). The dimension of V_b is typically in the order of $\mu\text{m}/\text{hour}$. During etching, in practice, units of μm are usually etched from each side of the detector (for example, in the case of TASTRAK detectors and standard processing during neutron measurement, it is approximately $12 \mu\text{m}$ from each side). The bulk etch rate depends on the detector material, the composition of the etching solution, and its parameters. The track etch rate also depends on the radiation damage to the detector material, and thus on the type and energy of the incident particle. The ratio of V_b and V_t defines the etching ratio V (-), also called sensitivity, and it also defines the critical angle of etching δ_c (rad),

$$\sin \delta_c = \frac{1}{V} = \frac{V_b}{V_t}, \quad (3)$$

which is the maximum angle at which a particle can impinge on the detector surface to create an etched track. It was found that the sensitivity V does not depend on the etching conditions and is constant for a given combination of detector material, type of incident particle, and its energy. This property has been intensively studied and the sensitivity values V for different particles have been measured, and the corresponding functions [17] have been proposed. These functions are used in programs such as TRACK_TEST [18], TRACK_P [19], and Neutron_CR-39 [20] to calculate the parameters of etched tracks from α particles, protons, and recoiled protons in the detection of fast neutrons, respectively. It should be noted that, given the findings of the thesis, where the etching properties of PADC detectors differed for individual detectors batches from the same manufacturer, this must be considered when using sensitivity functions V , especially in the case of light ion detection, i.e., protons.

Both bases and acids can be used for etching. PADC detectors are usually etched with NaOH or KOH solutions with a molar concentration between 1 M and 12 M, temperatures range between $60 \text{ }^\circ\text{C}$ and $98 \text{ }^\circ\text{C}$, and the etching time t (s) can be from tens of minutes to hours, depending on the type of radiation detected and the method of track imaging. The manufacturer of TASTRAK detectors recommends etching in a 6.25 M NaOH solution. When processing detectors after neutron measurements, the solution temperature is $85 \text{ }^\circ\text{C}$ and the etching time is 2 hours and 50 minutes; when measuring radon activity concentration, the solution temperature is $98 \text{ }^\circ\text{C}$ and the etching time is one hour. After etching, the detectors are rinsed in demineralized water, then neutralized for half an hour in a 2% solution of glacial acetic acid and rinsed again for 10 minutes in demineralized water. These conditions were applied for most of the experiments carried out as part of the thesis.

Since the dissertation focused mainly on the detection of fast neutrons, the energy dependence of the number of etched tracks per incident neutron was simulated. The simulation was performed using a combination of the Neutron_CR-39 and MCNP6.2 programs [21] (which will be described in the following section). The energy dependence was simulated independently for the front (closer to the

radiation source) and back sides of the 1.5 mm thick PADC detector etched under the conditions used at STU, as shown in Fig. 1.

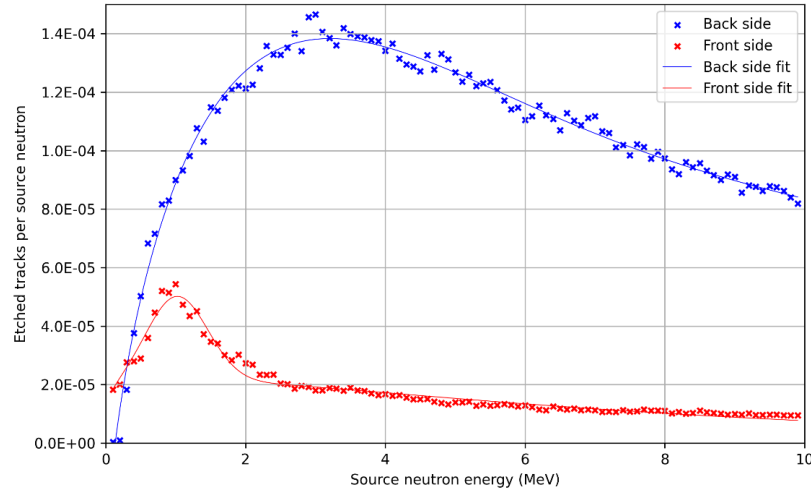


Figure 1: Energy dependence of the number of etched tracks per source neutron for the front (red) and rear (blue) sides of the PADC detector, simulated using a combination of the Neutron_CR-39 and MCNP6.2 programs [22].

For both the front and back sides, the simulated data was interpolated using an empirically derived function

$$f(E) = A_f \cdot E^{B_f} \cdot e^{-C_f E} + D_f \cdot e^{-\frac{(E-\mu_f)^2}{2\sigma_f^2}}, \quad (4)$$

Where E is the energy of the original neutron in MeV. The parameters of the best fits are given in Tab. 1.

Parameter	Back	Front	Unit
A_f	1.64E-04	2.51E-05	1/MeV
B_f	0.709	0.214	-
C_f	0.193	0.168	1/MeV
D_f	-6.89E-05	2.89E-05	-
μ_f	5.035	1.019	MeV
σ_f	4,562	0.438	MeV

Table 1: Parameters of the best fits of Eq. 4 for the front and rear sides of PADC detectors used at STU [22].

A mixing station for the etching solution was constructed at STU (for easier and faster preparation of the solution) as part of the thesis in cooperation with P. Mikula, consisting of a 3D-printed NaOH dispenser powered by a motor controlled by an Arduino module. The dispenser is regulated by a thermistor, which transmits information on the temperature of the solution to the evaluation module. The second part consists of a 25 l container for preparation of the solution and a mixer powered by a DC motor, whose speed is controlled by a voltage divider. Both parts are electrically isolated from each other; if the temperature of the solution rises, the supply of NaOH is interrupted, but mixing continues. This device enabled the time reduction in the preparation of the solution from 2 working days to approximately 3 hours.

Although simplified models [23], which depict the etched track as a cone, are sufficient to provide an idea of the shape of the etched track, the actual etched track has a cone-like shape, where V_t is variable along the path of the incident particle. Fig. 2 shows the shape of the wall of the etched track when the particle is incident in parallel to the x-direction. L (m) is the length of the particle's path in the detector, δ (rad) is the angle between the wall of the etched track and the path of the incident particle. The angle can be expressed for each point x_0 (m) as

$$\sin \delta(x_0) = \frac{1}{V(x_0)} = \frac{V_b}{V_t(x_0)}. \quad (5)$$

The search for the shape of the etched track (x and y coordinates of the etched track wall) leads to a solution based on the differential equations. Programs such as TRACK_P and Neutron_CR-39, used to simulate etched tracks, are based on solving these equations.

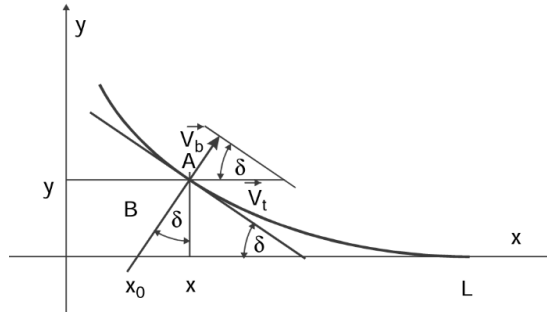


Figure 2: Two-dimensional sketch of the wall of an etched track [23].

Etched tracks appear as ellipses and ellipse-like shapes on the surface of the detector, and the shape of the track can be described using the major and minor axes of the ellipse. When a particle is incident perpendicularly, the track is circular in shape, in which case it is permissible to refer to the diameter of the track.

If the etching takes longer than required to reach the end of the latent track, so-called over-etching of the track may occur. In this case, etching continues in all directions of the track with the rate of V_b , resulting in a gradual loss of track properties when viewed under a microscope. An example of such a track is shown in Fig. 3, obtained by simulation in TRACK_P.

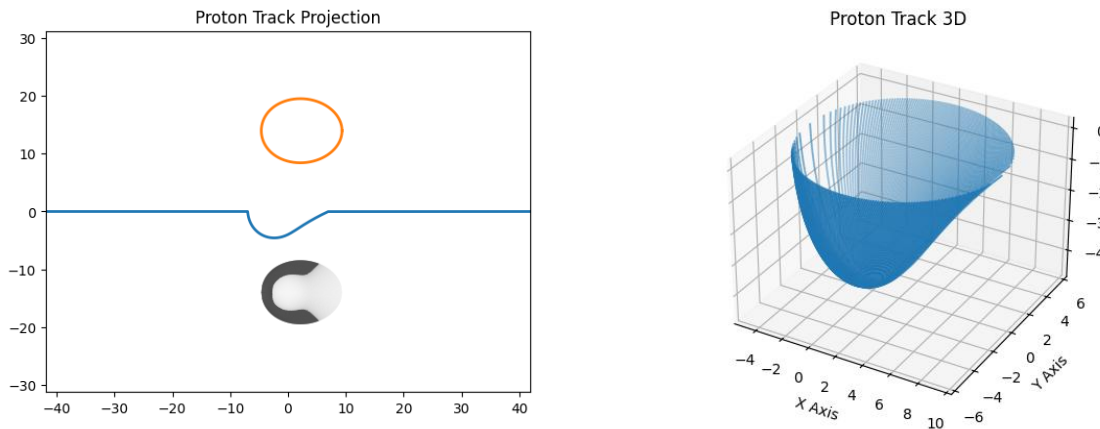


Figure 3: Simulated shape of an etched track for a 0.8 MeV proton, incident at an angle of 30°, etched with 6.25 M NaOH at a temperature of 85 °C for 2 hours and 50 minutes.

There are several methods for determining V_b [11]. The direct method, based on the difference in detector thickness before etching d_1 (m) and after etching d_2

$$V_b = \frac{d_1 - d_2}{2t} \quad (6)$$

is, according to [24], not reliable for short etching times; the authors recommend not using this method for etching times shorter than 2.5 hours. Another, gravimetric, method determines V_b using the difference in weight before etching m_1 (kg) and after etching m_2

$$V_b = \frac{m_1 - m_2}{2A_d \rho t}, \quad (7)$$

where A_d (m²) is the size of the etched area of the detector and ρ (kg/m³) is the density of the detector material. One of the most widely used methods is the measurement of tracks from fission fragments

$$V_b = \frac{D}{2}, \quad (8)$$

where D (m) is the diameter of the track from the fission fragment. For this purpose, detectors are exposed to ²⁵²Cf; only tracks from particles that are incident on the detector surface perpendicularly are

relevant for the calculation. Since, in addition to fission fragments, α particles and neutrons are also emitted. In the thesis, D and V_b were determined using the code that allowed for plotting the frequencies of sizes of D . The individual peaks of the histogram then corresponded to tracks from neutrons, α particles, and fission fragments, respectively. Interpolating the peak from fission fragments with a Gaussian allowed for the determination of the value D , which corresponded to the mean value μ , and the uncertainty, which corresponded to the standard deviation σ .

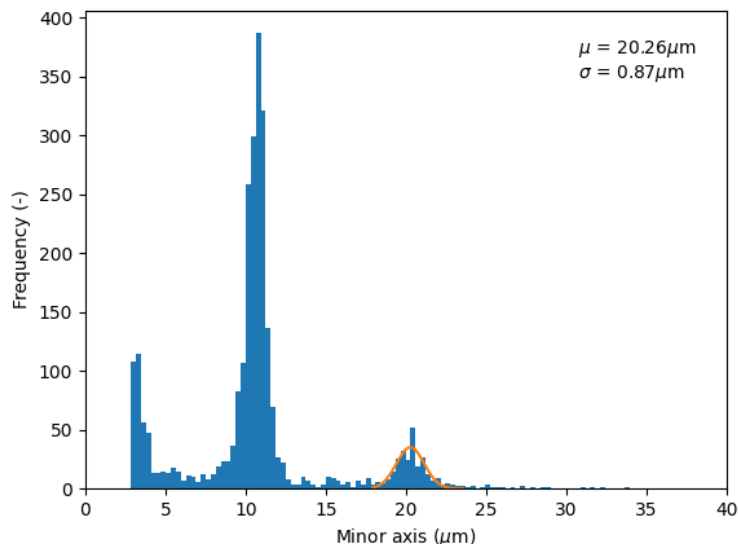


Figure 4: Histogram of sizes of minor axis of tracks from the PADC detector after irradiation with ^{252}Cf . The first peak corresponds to fast neutrons, the second to α particles, and the third to fission fragments. The graph also shows the Gaussian curve fit for the peak from fission fragments [25].

3.7. Evaluation

The TASLImage system from the manufacturer of the TASTRAK detectors is used at STU to analyze PADC detectors. The system consists of an optical microscope with 20x magnification, connected via a CCD camera to a computer with software for microscope control. The system allows automatic scanning of up to 49 detectors with dimensions of $2.5 \times 2.5 \times 0.15 \text{ cm}^3$ used at STU for neutron detection, or 56 detectors with dimensions of $2.5 \times 2.0 \times 0.15 \text{ cm}^3$ used to measure radon activity concentration. The system takes 80 images of the detector surface, and it automatically evaluates them. A folder with photos, two binary files, one with the extension TRK containing information on all detected events between $3 \mu\text{m}$ and $40 \mu\text{m}$ in size, and the other with the extension tmp containing the same information about selected candidate events for etched tracks are assigned for each detector. The system allows saving information from tmp in csv format. Table 2 contains a list of individual parameters of the registered events. The system also provides information on the density of the detected tracks (number of tracks per 1 cm^2) and the corresponding dose value in mSv, including the corresponding uncertainty, expresses as the standard deviation. To convert the track density to dose, the user can rely on the internal calibration of TASLImage, or the data can be calibrated by the change of the name of the relevant detector file in the folder. The user is thus able to assign a specific measured dose value to a given detector. If the detector is damaged or if there is dust or dirt on the surface, the system marks the detector data with an asterisk, and the resulting value is considered incorrect at STU.

Since the coordinates of events in the files are relative to the coordinate system given by the internal settings of TASLImage, the system was decoded as part of the thesis. Based on the corresponding findings, Samuel Gibala has created a Python code named CAT-code (Circle Around Track), which allows the localization of individual events from a csv file on the corresponding photo.

As part of the thesis, a code for transcription of TRK and tmp binary files into csv files was created to enable work with these files. Since the data used in the thesis were collected continuously, a folder structure was proposed to allow easy navigation through the stored data. Over 13 TB of data has been stored since 2022, corresponding to the processing of approximately 5.400 detectors, considering 2,400 MB per detector when scanning both sides. The data are being used in the EU PANDORA project [26].

<i>Label</i>	<i>Description</i>
X,Y	Coordinates of the track-spot centroid (μm)
XT/MJ	Projected length of the track/Major axis of the track-spot fitted ellipse (μm)
MIN	Minor axis of the track-spot fitted ellipse (μm)
GREY	Gray level value averaged over the whole track-spot (-)
SYMM	Track-spot symmetry along its major axis (-)
CONV	Track-spot convexity along its major axis (-)
SHARP	Sharpness of the track-spot edge (-)
FOCUS	Measure of the focus of a track (-)
AREA	Actual area of the track-spot (μm^2)
A1	Ratio of the actual track-spot area and the predicted area of the fitted ellipse (-)

Table 2: Parameters of events registered by the TASLImage system [27].

3.8. Codes developed at STU

The codes described in this section were developed within the thesis to ease and to standardize the data processing from the PADCs.

SW4A: PADC (SoftWare for Analysis of ionizing radiation measurement data from PADC detectors) was created using the Python programming language. The code structure was presented at the ELITECH24 doctoral student conference (where the author of the thesis received an IEEE award) and was published in the proceedings [25]. The code has its graphical user interface, allowing for easy operation. It is divided into several modules that enable the application of different analysis methods according to the needs of a given experiment. The *Plot* module allows the plotting of mutual dependencies of parameters from Tab. 2 for individual detectors. In the *Histograms* module, it is possible to plot the frequencies of occurrence of a given quantity from Tab. 2 for selected detectors. The *Etching parameters* module is used to calculate the etching rate V_b according to Eq. 6-8. The *Multiple analysis* module serves to process results in the case of multiple scans of a single detector. In such a case, it assigns the relevant results to each other and calculates the resulting value. The *Principal component analysis* module combines the statistical method of principal component analysis (PCA) and the HDBSCAN (Hierarchical Density-Based Spatial Clustering of Applications with Noise) clustering mechanism to sort data obtained from PADC detectors. The data are plotted in a new coordinate system where the x, y, and z axes represent the three principal components for the given problem. The data are then classified into individual clusters using HDBSCAN. This approach was tested in the thesis on the data from measurements of the angular response of PADC detectors in the detection of α particles [28] or in the detection of neutrons from a Pu-Be neutron source [29].

KOSTKAcodes [22] is another code written in Python, developed as part of the thesis. It was designed to project data from PADC detectors installed in the KOSTKA device onto a spherical surface, allowing the determination of the spatial distribution of neutrons emitted from the source installed inside the KOSTKA device. The code is based on the Monte Carlo pseudo-random Lehmer number generator, which allows the creation of unique pairs of azimuth angle ϕ and polar angle θ , indicating a random direction from the center of coordinates. The polar coordinates of the pseudo-random unit vector are then converted to

Cartesian coordinates. The output from the KOSTKA device has to be organized into an Excel table so that each area occupied by the detector is assigned the boundaries of that area and the measured density of etched tracks (or the measured dose) before the start of the simulation. The coordinate at which the vector intersects the wall of the KOSTKA device is calculated for each pseudo-random vector. If a detector was located at the position of intersection, its value is added to the corresponding element of the solid angle. At the end of the simulation, the total value for each element of the solid angle is divided by the number of vectors that passed through that element. The simulation results can be displayed as a 3D graph and are also exported in table format for further processing.

3.9. Other programs

The following paragraphs describe the other programs used within the thesis.

MCNP (Monte Carlo N-Particle® Transport Code System) is a tool enabling the Monte Carlo simulations of particle transport. Version 6.2 offers tracking of heavy charged particle transport, which is advantageous for simulations in the phase of designing experiments with PADC detectors. In the thesis, MCNP was used to design experiments in which the proton flux through the surface of the PADC detector was monitored under given conditions using tally F2. Another use was the creation of input files for the Neutron_CR-39 program from the PTRAC output of MCNP, which contains a record of all interactions of the monitored particles, including their coordinates.

SRIM (Stopping and Range of Ions in Matter) was used to simulate the range of ions in matter. It can be used, for example, to design the radiators or degraders for individual experiments.

Neutron_CR-39 is a program written in FORTRAN and developed at the University of Kragujevac. The program was used for Monte Carlo simulation to determine the number of etched tracks from recoiled protons as a result of exposing a PADC detector to a neutron source under given etching conditions. As part of the thesis, the original program was modified to correspond to the experimental conditions at STU. The cylindrical Am-Be neutron source was rotated so that the axis of the cylinder pointed towards the PADC detector in the original version. After modification, the source was rotated so that the axis of the cylinder was vertical (i.e., parallel to the PADC detector), as this arrangement corresponds to the real experiments at STU. Files with spectra of other neutron sources, such as Pu-Be, were also added. A simplified calculation of the minor axis of the ellipse was added, and upper and lower limits for accepting etched tracks were set, corresponding to the TASLImage settings (from 3 μm to 40 μm). The counting of the etched tracks on the front and back side was separated. After modification, the program also allows the use of simulation results from the MCNP program (specifically from the PTRAC output) instead of its own simulation of latent track formation (from neutron interactions with hydrogen protons in the PADC detector). The reason for this step is that the Neutron_CR-39 program relies on the isotropic distribution of recoiled protons when calculating the direction of the recoiled proton, which could lead to a distortion of the simulation result.

Track_P is a program developed by the same team of authors as Neutron_CR-39, but this program is used to simulate the shape of etched tracks from protons, depending on the energy and angle of incidence for given etching conditions. The program provides the parameters of the etched track (major and minor axis, track depth, and the dark area of the track) as well as a visualization of the etched track.

TRACK_TEST is a program that performs the same function as Track_P, but for incident α particles. The visualization of the resulting etched track is simplified compared to the output of the Track_P program.

4. Results

This chapter briefly summarizes selected results of experiments conducted as part of the thesis. Most of the experiments described in the thesis have been published or submitted to journals prior to the submission of the thesis. The first four selected experiments were designed to verify the properties of PADC detectors and to propose the appropriate methodology, while the last two experiments represent practical applications of these detectors.

4.1. Acceptance testing with Pu-Be neutron source

The work described in [16] was carried out in cooperation with the Slovak Institute of Metrology (SMU). The aim was to verify the response of PADC detectors and the TASLImage system in the neutron field of a Pu-Be neutron source. The experimental setup is shown in Fig. 5. In the experiment, the Pu-Be neutron source of IBN 26 type, serial number 033, with the emissivity of $1.995E7$ neutrons/s/ 4π (on the reference date 12/21/2021), and a source radius of 2.1 cm.

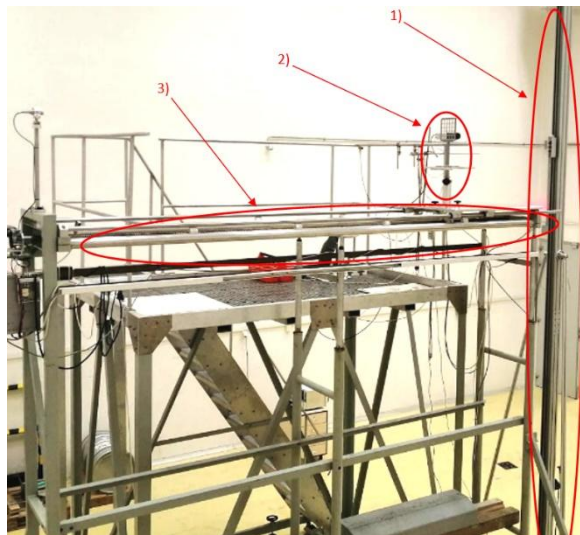


Figure 5: Experimental setup at SMU with 1) a column for remote-controlled movement of the radiation source, 2) a holder for PADC detectors, and 3) a measuring bench [16].

Two sets of detectors were irradiated in the experiment. The first set of 250 detectors from five different sheets from a single batch was irradiated within 14 days in April 2022. The ambient dose equivalent at the detector position ranged from 0.144 mSv to 14.989 mSv (values of $H^*(10)$ with uncertainties are given in Tab. 3). Detectors from this set were transported in thin polyethylene bags. After irradiation, they were randomly divided into five groups of 49 detectors and etched in 6.25 M NaOH at 85 °C for 2 hours and 50 minutes and then neutralized. Scanning took a month.

A second set of 293 detectors (among which 18 detectors were not irradiated for background monitoring) from five different sheets from the same batch was irradiated during 14 days at the beginning of September 2022. Thick vacuum polyethylene bags were used to transport the detectors. For etching, the detectors were divided into three groups of 98. Scanning also took a month.

The analyses included several tests. The initial sensitivity test consisted of two parts. In the first part, photos of the surface of detectors exposed to 3.027 mSv were randomly selected and visually compared. If there would be significant differences between the photos, the detectors from the corresponding sheet would be excluded from further analysis. Fig. 6 shows a comparison of three random photographs of detectors and the corresponding graphs, in which the coordinates of the etched tracks for each detector are plotted. All sheets were accepted for further analysis.

t (h)	Set 1		Set 2		N
	H*(10) (mSv)	uH*(10) (mSv)	H*(10) (mSv)	uH*(10) (mSv)	
0.57	0.144	0.007	0.144	0.007	25
3.97	1.009	0.047	1.009	0.047	25
7.95	2.018	0.095	2.018	0.095	25
11.92	3.027	0.142	3.027	0.142	25
17.59	4.468	0.21	4.468	0.21	25
23.84	6.053	0.284	6.053	0.284	25
31.78	8,071	0.379	8.071	0.379	25
39.73	10,089	0.474	10.089	0.474	25
45.41	-	-	11.53	0.541	25
49.38	12.539	0.589	12.539	0.589	25
59.03	14.99	0.704	14.99	0.704	25

Table 3: Irradiation times, H*(10), corresponding uncertainty, and number of irradiated detectors for both sets [16].

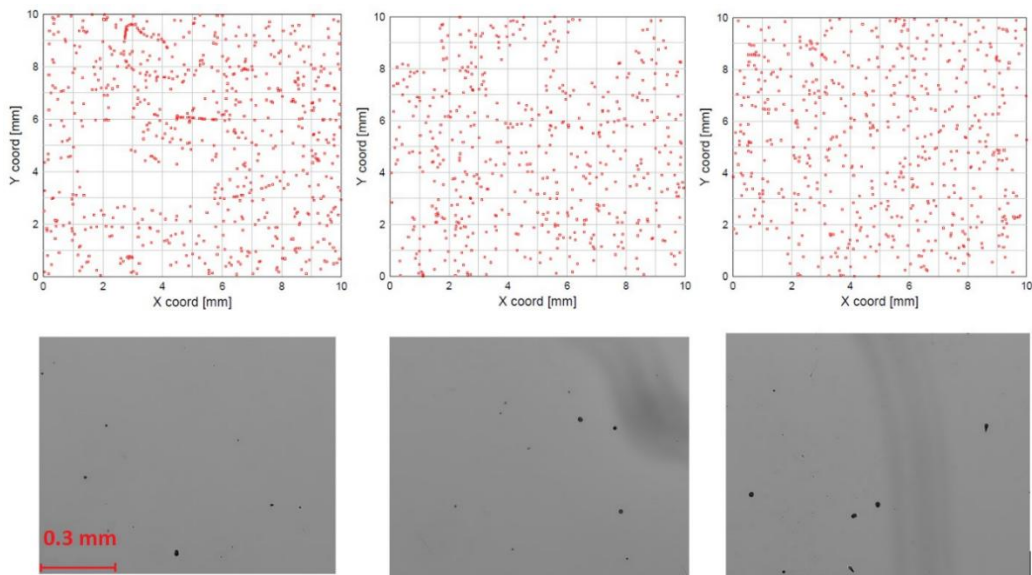


Figure 6: Three randomly selected photographs of detectors and the corresponding track coordinates for each detector [16].

The next part of the initial sensitivity test consisted of calculation of the sensitivity according to

$$sensitivity = \frac{etched\ tracks\ density}{H^*(10)\text{-}area} \quad (9)$$

The average sensitivity was determined for each sheet and then compared with the calibration value from TASLImage for the given etching. The relative values, determined as the ratio of the average sensitivity and calibration value, were compared. Since all values agreed within the uncertainties, all sheets were accepted for further analysis in the second part of the sensitivity test.

The experiment also included the determination of detection limits based on the background signal from 18 unirradiated detectors from the second set. The average detection limit value was 0.11 mSv, while the value specified by the manufacturer of TASTRAK detectors is 0.1 mSv. The data from the first set of detectors were used to verify the effect of the calibration value selection on the TASLImage system output. The data were calibrated sequentially in this test, according to two detectors irradiated with the same H*(10) (see Tab. 3). The results showed that, apart from calibration value close to the detection limit, the choice of calibration value had no significant effect on the system response.

Confidence intervals were defined for data from both experiments and compared with the limit values according to the ICRU recommendations for H*(10) measurements. The results are shown in Fig. 7, which clearly shows that all results were accepted within the given limits.

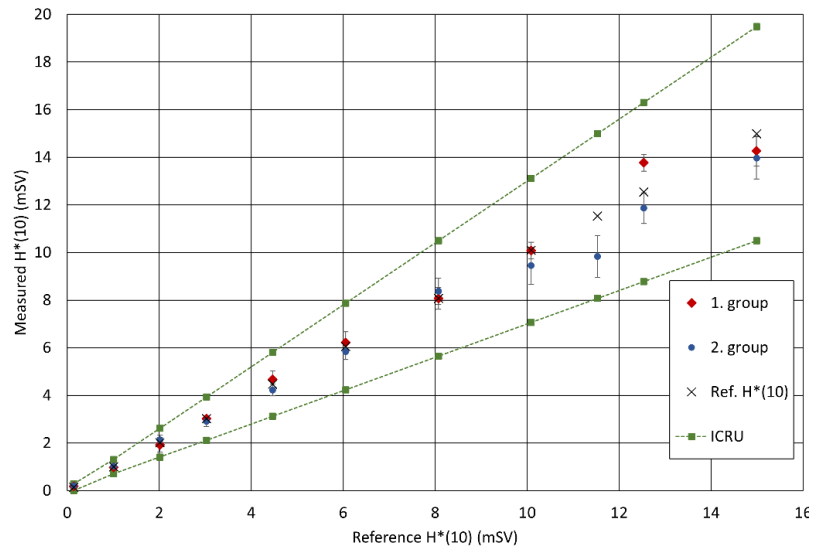


Figure 7: Confidence intervals for both sets of detectors, compared with the limit values according to the ICRU recommendation [16].

The results for the second set of detectors were averaged for each etching separately and compared with each other and with confidence intervals in Fig. 8. Also, the bulk etch rate and the thickness of the removed layer was measured for selected detectors using a gravimetric method according to Eq. 7. The thickness of the removed layer was 11.74 μm , 11.84 μm , and 11.01 μm for the first, second, and third etching, respectively. The data in Fig. 8 show a difference between the results for the third etching cycle, for which a different thickness of the etched layer was measured. Based on this observation, an experiment, which is described in the next section, was designed.

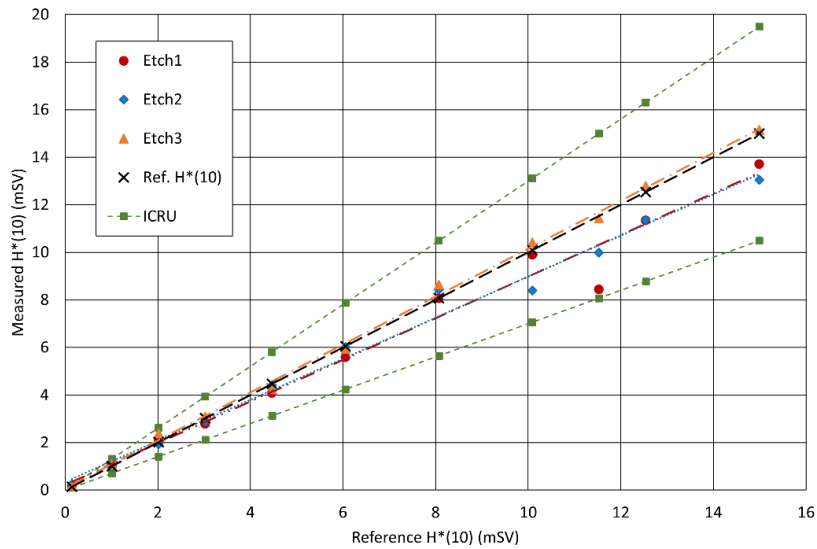


Figure 8: Confidence intervals and $H^*(10)$ values averaged for individual etchings [16].

The study presented focused on the evaluation of detectors according to several approaches. In terms of sensitivity tests, all sheets were accepted for evaluation within the experiment. A new approach to handling detectors during transport was established, involving thick PE vacuum bags. It was shown that detectors exposed to $H^*(10)$ above the detection limit can be used for calibration in the TASLImage system. The results obtained from the analysis of PADC detectors were compared with the recommendations given by the ICRU, and the results were evaluated as satisfactory. The possible effect of a small change in etching conditions on the response of the detectors was shown, based on which the following experiment was proposed.

4.2. Etching Time Effects on Fast Neutron Response in PADC Detectors

The follow-up experiment was again conducted in cooperation with SMU using the same Pu-Be neutron source. The aim of the experiment was to evaluate the effect of change in the etching time of the detectors on the response of the system. The data described in an article [30], which was submitted to the journal Radiation Physics and Chemistry.

The detectors were exposed to six different reference levels of $H_r^*(10)$ (see Table 4), with 150 detectors irradiated each time, to evaluate the effect of etching. To achieve homogeneous exposure, the detectors were installed at a distance of 180 cm from the neutron source. The 900 detectors in total were irradiated and evenly divided into ten groups for etching. Another 20 detectors were irradiated with fission fragments from ^{252}Cf at the Polytechnico di Milano to measure the bulk etch rate using tracks from fission fragments. Two detectors exposed to fission fragments were added to each etching group.

t (h)	$H_r^*(10)$ (mSv)	$u[H_r^*(10)]$ (mSv)
12.68	1.009	0.076
38.03	3.027	0.228
76.06	6.053	0.457
101.4	8.071	0.609
126.76	10,089	0.761
157.55	12.539	0.946

Table 4: Overview of irradiation times and corresponding $H^*(10)$ values, including uncertainties [30].

The etching cycles were designed based on the recommended conditions (NaOH with a molarity of 6.25 M and a temperature of 85 °C, etching time 2 h and 50 min, neutralized by 30 min of rinsing in glacial acetic acid and 10 min of rinsing in demineralized water). Based on the assumption that the corresponding thickness of the removed layer is 12 μm and that the relationship between the thickness of the etched layer and the etching time is linear, the etching times were proposed to achieve 1 μm increments of the thickness of the removed layer. The neutralization times were adjusted accordingly. Tab. 5 contains an overview of the expected etched layer thicknesses h_e , measured values h_m , including uncertainties u_{hm} , and corresponding etching times t_E , neutralization times in acid solution t_k , and in demineralized water t_d .

h_e (μm)	h_m (μm)	u_{hm} (μm)	t_E (min)	t_k (min)	t_d (min)
8	8.13	0.49	113	20	7
9	9.1	0.29	128	23	8
10	10.1	0.34	142	25	8
11	11.11	0.33	156	28	9
12	11.84	0.37	170	30	10
13	13.15	0.39	184	33	11
14	13.94	0.81	199	35	12
15	14.69	0.5	213	38	13
16	16.19	0.4	227	40	13
17	16.68	0.6	241	43	14

Table 5: Overview of thicknesses of the removed layers and corresponding etching and neutralization times [30].

For individual expected thicknesses of the removed layer, a theoretical PADCs response was simulated using a combination of the Neutron_CR-39 and MCNP6.2 programs. Fig. 9 shows the resulting dependence of the number of etched tracks created per one latent track on the thickness of the etched layer. It shows that for both the front and back sides of the detectors, the density of etched tracks should increase with increasing thickness of the removed layer.

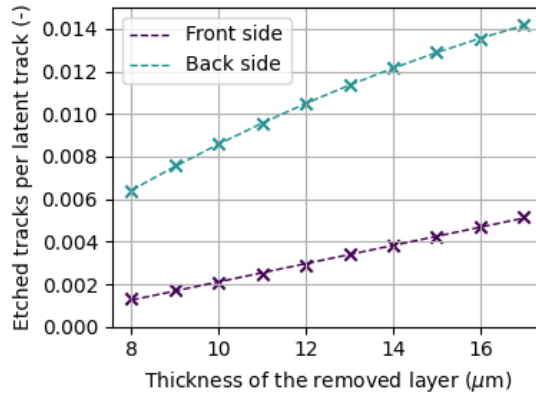


Figure 9: Simulated response of PADC detectors based on combination of the Neutron_CR-39 and MCNP6.2 programs [30].

For each set of etched detectors, the average value of the etched tracks density was obtained, with the standard deviation considered as the uncertainty. The energy dependence of the etched tracks density for the front sides of the detectors is shown in Fig. 10. The same dependence for the back sides of the detectors is shown in Fig. 11.

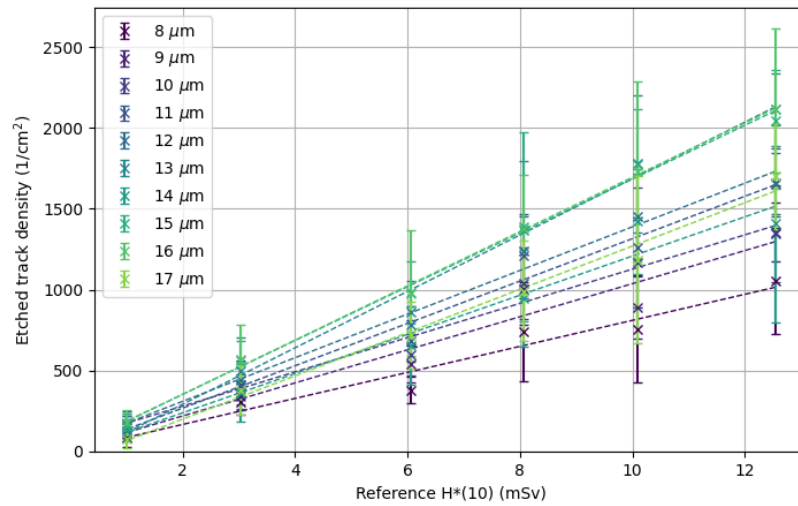


Figure 10: Energy dependence of the density of etched tracks for different expected thicknesses of the removed layer on the front side of the detectors [30].

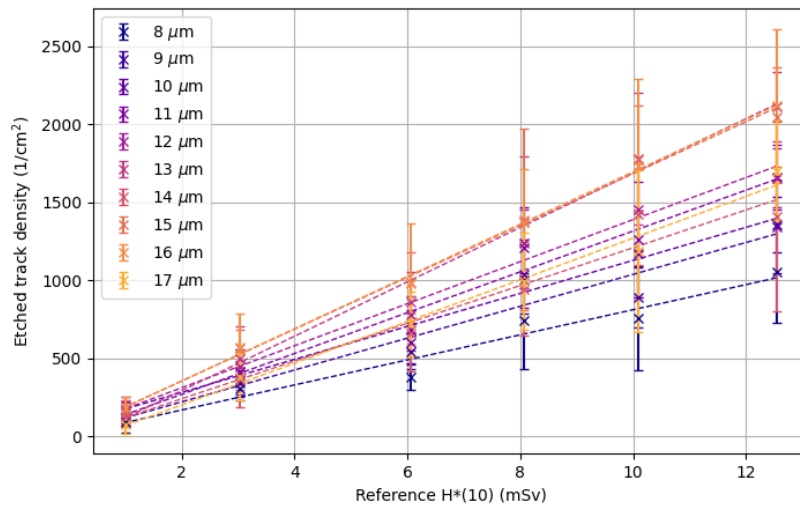


Figure 11: Energy dependence of the density of etched tracks for different expected thicknesses of the removed layer on the back side of the detectors [30].

The individual points were interpolated using linear regression, and the corresponding regression metrics are summarized in Tab. 6 for individual interpolations. The slopes k of the individual interpolations were plotted in Fig. 12 and interpolated using a second-order polynomial for further analysis. The metrics, such as the coefficient of determination R^2 , the standard deviation of the interpolation σ , the relative deviation of the interpolation slope rel. (calculated as σ/k), and the p-value, show that the data were highly linear in all cases and that linear regression was therefore a suitable method for data interpolation.

h_e	Front					Back				
	k	R^2	σ	rel.	p-value	k	R^2	σ	rel.	p-value
8.13	80.43	0.956	8.64	0.11	7.40E-04	355.45	0.995	12.97	0.04	1.05E-05
9.10	102.21	0.94	12.88	0.13	1.37E-03	444.57	0.995	15.62	0.04	9.06E-06
10.10	105.86	0.972	8.97	0.08	2.95E-04	428.57	0.996	14.24	0.03	7.26E-06
11.11	130.92	0.976	10.33	0.08	2.23E-04	506.46	0.999	6.32	0.01	1.45E-07
11.84	134.82	0.985	8.40	0.06	8.82E-05	571.01	0.999	9.00	0.02	3.70E-07
13.15	174.38	0.991	8.52	0.05	3.37E-05	571.71	0.991	27.77	0.05	3.29E-05
13.94	121.11	0.959	12.56	0.10	6.48E-04	511.57	0.997	13.42	0.03	2.83E-06
14.69	166.27	0.994	6.27	0.04	1.20E-05	531.95	0.995	18.15	0.03	8.07E-06
16.19	167.79	0.998	3.80	0.02	1.57E-06	508.43	0.996	15.91	0.03	5.71E-06
16.68	133.71	0.988	7.32	0.05	5.30E-05	422.83	0.994	16.05	0.04	1.24E-05

Table 6: The metrics of the linear regressions for both sides of the detectors [30].

A comparison of the change of slope as a function of the thickness of the removed layer showed a linear increase to a value of approximately 12 μm for both the front and back sides of the detectors. In the case of the front sides, the slopes for larger thickness of the removed layer were scattered, while a decrease was observed for the back side. Since 12 μm corresponds to the recommended etching procedure for TASTRAK detectors in neutron detection with TASLImage, the discrepancy between experimental data and simulations is most likely due to TASLImage internal track-acceptance settings. Changing the etching time alters not only the thickness of the etched surface layer, but also the track shape, which at longer etching times may no longer satisfy the TASLImage acceptance criteria.

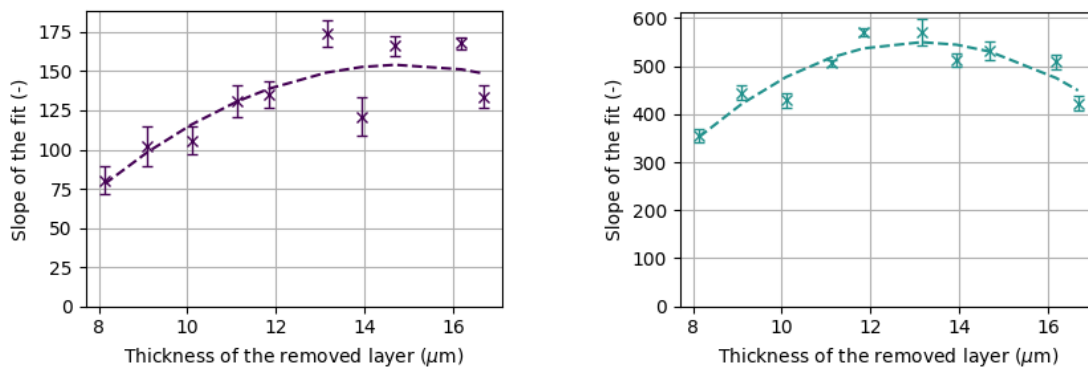


Figure 12: Dependence of the fit slope from Table 6 on the thickness of the etched layer for the front (left) and rear (right) sides of the detectors [30].

The data in Fig. 12 were fitted with the second-order polynomials described by the equations

$$k = -1.68 \cdot h^2 + 49.88 \cdot h - 216.57 \quad (10)$$

for the front side of the detectors and

$$k = -7.94 \cdot h^2 + 208.38 \cdot h - 817.40 \quad (11)$$

for the back side of the detectors. These equations may be used in the future as a correction of the measured data in the case of deviation in the thickness of the removed layer.

4.3. Combination of PADC and radiator for neutron radiography

Another experiment in collaboration with SMU focused on the combination of PADC detectors and radiators, with the main goal of verifying the response for the design of an experimental setup for fast neutron radiography using PADC detectors. The study was presented at the APCOM24 conference and published in [31].

Although the use of a D-D neutron source is planned for neutron radiography at STU, since it was not available at STU at the time of the experiment, a Pu-Be neutron source at SMU (the same as in previous experiments) was used instead.

Various thicknesses of HDPE were proposed as radiator, and the use of Kapton tape was also verified. The change in detector response when using a radiator was simulated in MCNP. The simulation was simplified, considering a surface neutron source on the radiator layer, under which was a layer of PADC detector. The proton flux was monitored (through tally F2) on the surface of the detector before etching and at a depth of 12 μm (corresponding to the situation after etching) on both the front and back sides of the detector. HDPE radiators with thicknesses of 0.05 mm, 0.1 mm, 0.5 mm, 1.0 mm, 2.0 mm, and 5.0 mm and Kapton foil with a thickness of 0.05 mm were simulated. Fig. 13 shows the simulation results for the situation after etching (i.e., at a depth of 12 μm below the detector surface), which indicate that for the front side of the detectors and the neutron spectrum corresponding to the Pu-Be neutron source, it is most advantageous to use a 1.00 mm – 2.00 mm HDPE radiator. In the case of the back side, there was no significant difference between the radiators used.

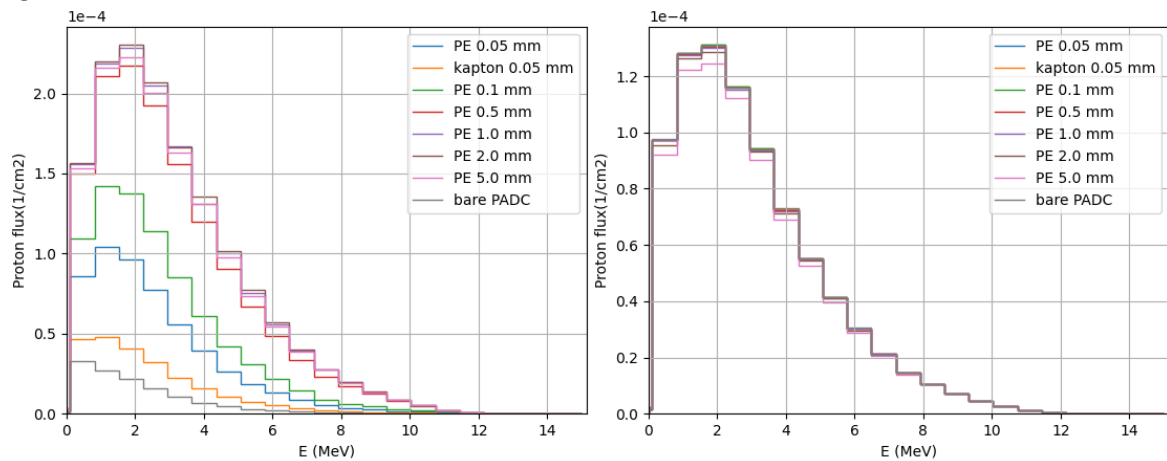


Figure 13: Simulated energy dependence of the proton flux[31].

The simulated data were experimentally verified. Industrially manufactured tapes (TESA 51134, TESA 51136, and Kapton tape) and HDPE manufactured at the Institute of Polymers of the Slovak Academy of Sciences (SAV) were used as radiators. An overview of the radiators used is given in Tab. 7.

Material	Type	Layer thickness (mm)	Number of layers	Total thickness (mm)
HDPE	TESA 51134	0.051	1	0.051
HDPE	TESA 51134	0.051	2	0.102
HDPE	TESA 51134	0.051	9	0.459
HDPE	TESA 5113	0.085	12	1.02
HDPE	SAV	1.00	1	1.00
Kapton	-	0.05	1	0.05

Table 7: Overview of the radiators used in the experiment [31].

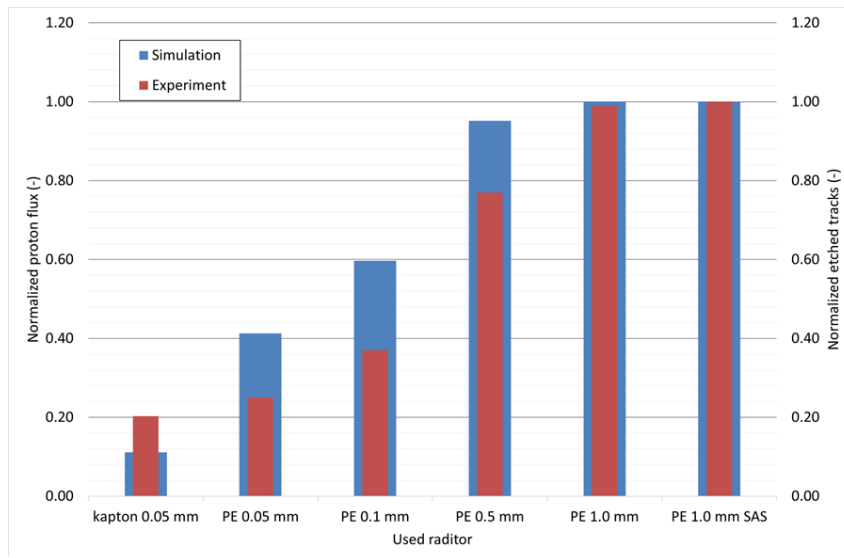


Figure 14: Comparison of normalized simulation results and experimental results for different radiators used [31].

Twenty-eight detectors were irradiated (four for each radiator configuration from Tab. 7 and four without a radiator) with the corresponding $H^*(10)$ value of 1.009 mSv. The detectors were etched according to the standard procedure used at STU. Fig. 14 shows a comparison of the normalized results of the MCNP simulation for a depth of 12 μm below the surface of the front of the detector and the normalized experimental results. All data were normalized to a value corresponding to an HDPE radiator with a thickness of 1.00 mm (in the case of experimental data from an HDPE radiator manufactured at SAV). The results show that the values obtained using HDPE manufactured at SAV and using the corresponding thickness of TESA tape were equivalent. Differences in the data may be due to variations in layer thickness caused by the layering of thin (0.051 mm) TESA tape.

4.4. PADC fading study

Further research within the thesis focused on the change in the response of detectors irradiated with fast neutrons with their storage after etching. The results of the nearly two-year-long experiment were presented at the RAP25 conference and submitted to the *European Physical Journal Special Topics* [32].

Detectors at STU are usually stored in a freezer at $-18\text{ }^\circ\text{C}$ before and after etching. In this experiment, 25 detectors were irradiated with a Pu-Be neutron source at SMU, delivered $H^*(10)$ was 10.03 mSv. The detectors were simultaneously etched according to standard conditions used at STU, scanned, and then randomly divided into three groups. The first group (Freezer) of 8 detectors was stored under reference conditions in a freezer, the second group (Black) was stored in an opaque bag at ambient temperature, and the third group (Sun) was exposed to sunlight at the ambient temperature in a transparent bag. The detectors were rescanned at random intervals.

Fig. 15 shows the change in the density of etched tracks for all storage conditions over time for the front side of the detectors. The graph shows a significant change in response for data obtained later than a year after the first analysis for all storage methods. The same trend was observed for the back side of the detectors. The same dependence is shown in Fig. 16 for the measured value $H^*(10)$ and the front side of the detectors. These data also show that after more than one year of storage, the response of the detectors was scattered compared to the original values. The same behavior was observed for the back sides of the detectors.

The results of the study show that the method of storage does not have a significant effect on the response of the detectors during the first year after etching. At the same time, however, the results

showed that the response of the system changes significantly during longer storage, and therefore the detectors should not be stored for longer than one year. Also, the TASLImage system itself has a significant effect on the results, thus, the data from the experiment will be further processed as part of ongoing cooperation with teams working on artificial intelligence and machine learning applications.

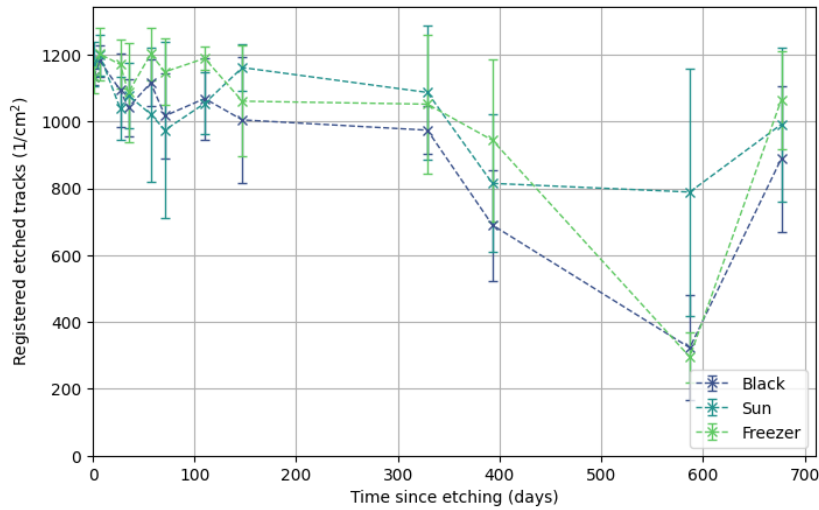


Figure 15: Change in the density of etched tracks over time for all storage methods and the front side of the detectors. The connecting lines are shown for better orientation in the graph [32].

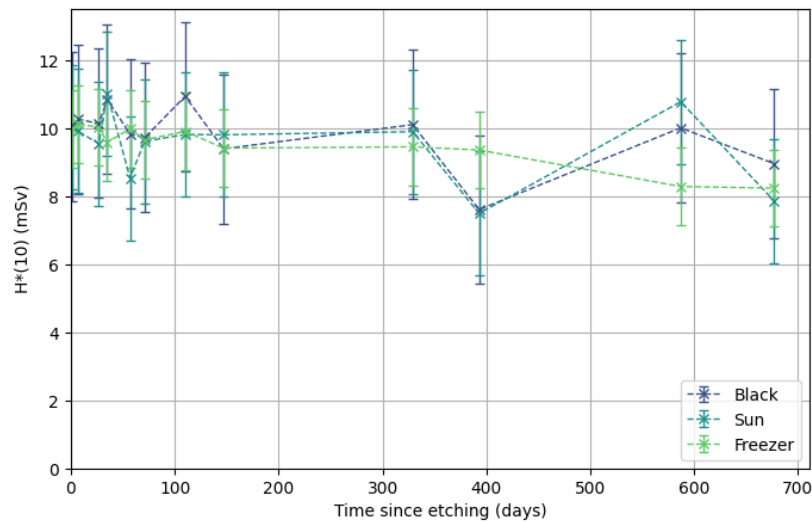


Figure 16: Change in the resulting $H^*(10)$ value over time for all storage methods and the front side of the detectors. The connecting lines are shown for better orientation in the graph [32].

4.5. First demonstration of neutron imaging using PADDC

The experiment presented at the RAP24 conference and published in [33] introduced the initial conditions for fast neutron radiography using PADDC detectors. The first demonstration was carried out on the TRIGA Mark-II experimental reactor in Vienna, in two channels – with fast (with a neutron spectrum with a maximum of approximately 1 MeV) and thermal neutrons. The results have not yet been published.

For radiography using fast neutrons, imaging was performed using a bare PADDC detector of $5 \times 5 \text{ cm}^2$, while for imaging with thermal neutrons, a BDD radiator was tested with the same dimensions of PADDC.

The experimental setup for imaging using fast neutrons is in Fig. 17, together with the resulting image obtained after 1.5 hours of exposure with a neutron flux of $6.7\text{E}5 \text{ neutrons/cm}^2/\text{s}$. The detector was etched for 2 hours and 50 minutes and then neutralized. The image was obtained by scanning with an aluminum background and subsequent processing in GIMP based on the conditions defined in [33].

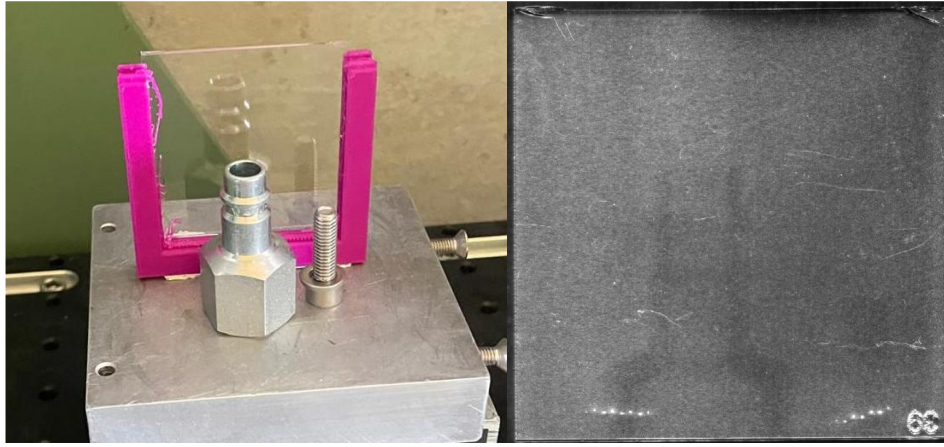


Figure 17: Experimental setup for radiography using fast neutrons and the resulting image.

The results obtained in the thermal neutron channel are shown together with the experimental setup in Fig. 18. The PADC detector was covered with a layer of BDD on the experimental channel side, enabling the detection of thermal neutrons via the (n,α) reaction. The exposure also lasted 1.5 hours, at a neutron flux of $1E5$ neutrons/cm²/s, which corresponded to a fluence of $8E3$ α particles/cm². The etching time was 20 minutes to achieve optimal conditions according to [34]. Although the α particle fluence was relatively low, the contours of the imaged objects are still visible in the resulting image, especially the part covered with the boron-doped filter on the left side of the experimental setup.

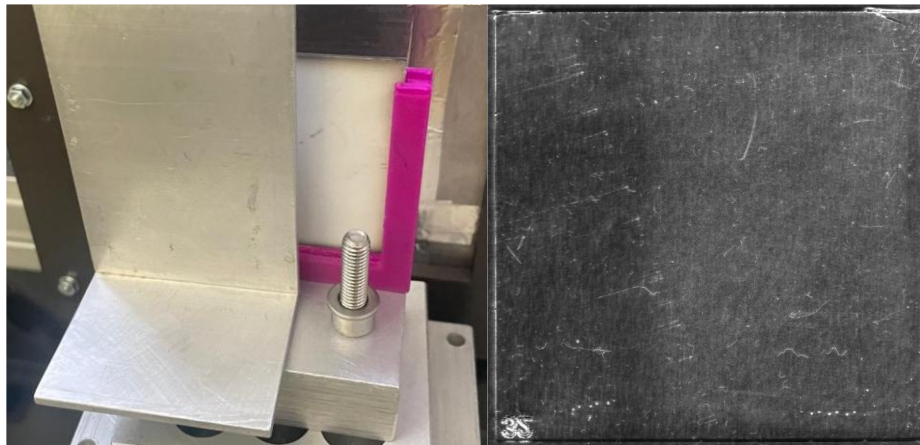


Figure 18: Experimental setup for thermal neutron radiography and the resulting image.

The first demonstration proved that it is possible to apply PADC detectors in neutron radiography; further research will focus on improving the parameters of the resulting images.

4.6. D-D neutron spatial distribution measurement

The last experiment presented in this text was devoted to measuring the spatial distribution of neutrons from the D-D reaction. The results were presented at the ANIMMA 2025 conference, partially published in the conference proceedings [35], and detailed results were submitted to the *IEEE Transactions on Nuclear Science* journal [22].

The presented work consisted of several parts. In the first part, a holder was designed to cover the spatial angle around the neutron source (in this work, around the experimental chamber installed at a TANDETRON accelerator). For this purpose, KOSTKA device (Fig. 19) was constructed, allowing the installation of 25 PADC detectors on each side (except for the necessary slots for the beam supply and other instrumentation). Furthermore, the KOSTKAcodes were designed in Python, enabling the data conversion from the cubic configuration in the KOSTKA to the surface of a sphere, enabling



Figure 19: The KOSTKA device installed around the experimental chamber [22].

determination of the spatial distribution of the measured quantity. The spatial distribution and change in neutron energy as a function of angle were simulated in the DROSG-2000 program [36]. Since the simulation showed a significant change in neutron energy with the angle, and since the response of PADC detectors is energy-dependent, the results were recalculated based on a simulation obtained from combination of the Neutron_CR-39 and MCNP (see Fig. 1) and based on simulated neutron energies from the DROSG-2000 program. An aluminum degrader (in Fig. 19) was designed for the first experiment based on a simulation in the SRIM program. Further simulations showed that all the protons from D-D fusion were stopped in the walls of the experimental chamber, and therefore the use of a degrader was not necessary.

Fig. 20 shows the results of an experiment with deuterons accelerated to an energy of 2.20 MeV. After passing through the experimental chamber window, the corresponding energy was approx. 0.926 MeV (according to SRIM). The data were compared with simulations in DROSG-2000 for 1 MeV deuterons. The results from both front and back sides corresponded to the simulated values. The deviation observed for angles above 130° was probably caused by the method of recalculation of values for the rear side of KOSTKA. If these values were lower, the response between approximately 60° and 120° would increase compared to the simulated values due to neutron scattering from the floor and ceiling.

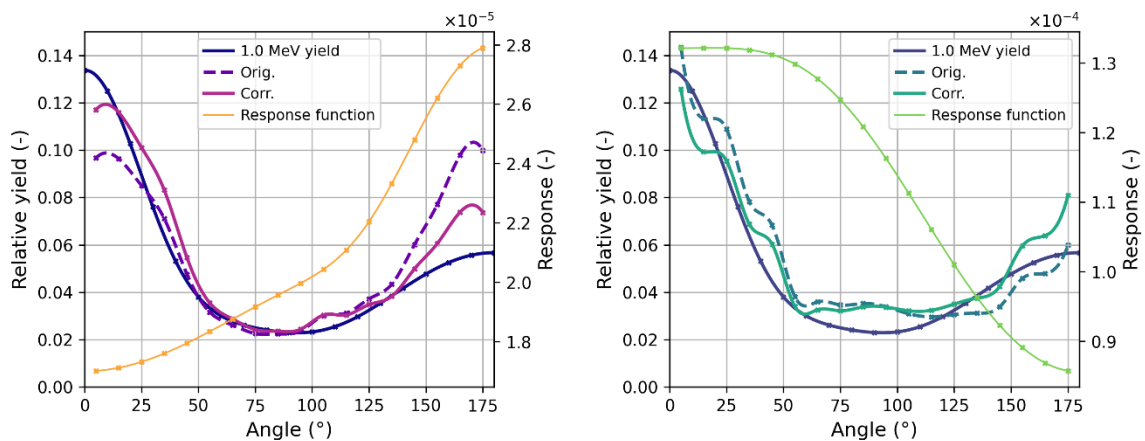


Figure 20: Comparison of the original results, the results recalculated based on the energy response of the PADC detectors, and the simulated reaction yield according to DROSG-2000 for the front (left) and back (right) sides of the detectors. The graphs also show the response function used to recalculate the original data [22].

The application of the KOSTKA together with the KOSTKAcodes for determination of the spatial distribution of the measured quantities was verified in this experiment. The resulting data corresponded to the simulated values. In further work, an alternative method of assessing values for angles where PADC detectors cannot be installed should be proposed.

5. Conclusion

The dissertation thesis aimed to develop a methodology for the use of PADC-type SSNTDs and to implement the proposed measures into the measurement of dosimetric quantities. Five topics of the dissertation were defined, focusing on various aspects of the use of PADC detectors. This text presented a brief overview of the function of SSNTDs and methods of their processing, including the software tools developed by the author of the dissertation thesis. Most of the experiments performed within the framework of the thesis were published. Four articles were under review when the thesis was submitted.

Many experiments were carried out within the dissertation with various sources of ionizing radiation, such as Am-Be and Pu-Be radioisotope neutron sources, but also other neutron sources such as D-D, or various channels of the TRIGA Mark-II experimental reactor. The detectors were also irradiated with ^{252}Cf , ^{241}Am and they were also used to measure the radon activity concentration in dwellings. The use of HDPE and Kapton radiators was proposed based on simulations and subsequently verified experimentally. An aluminum degrader was designed, but its use within the experiment was not necessary.

The etching processes at STU are based on recommendations of Tasl and were modified according to the purpose of the experiment. Participation in the EURADOS group allows STU, as a member, to compare data with laboratories using other etching processes. The change in response when changing the etching time was verified and a corresponding correction was proposed.

As for external conditions, a methodology was established for handling detectors throughout their lifetime, whether in terms of transport, handling, or storage (considering the experiments performed).

The Neutron_CR-39 code was debugged and modified so that its settings corresponded to the real experimental conditions at STU, including limits for the size of etched tracks. The code was also modified to allow simulation with input data obtained from MCNP. This enabled such simulations as the energy dependence of the response of PADC detectors.

Throughout the dissertation study, a number of experiments were conducted, on the basis of which a methodology for work with PADC detectors for various applications was compiled. Several software tools were developed to enable the processing of measured data.

Areas of potential future research were also identified within the thesis. One possible direction of research is the continuation of collaboration with teams of experts in artificial intelligence and machine learning fields who are currently working with data from past experiments within the PANDORA project. This cooperation could lead to more accurate recognition of etched tracks and thus to the reduction of the measurement uncertainty. The continuation in development of PADC detector analysis based on PCA and clustering mechanisms as proposed in the dissertation thesis, is closely linked to the previous area. This combination could also be suitable, for example, for the use of PADC detectors in nuclear forensic methods. Another direction is the neutron radiography, for which the initial conditions have been established and the first demonstration has been carried out. The use of PADC detectors in the dissertation has also proven successful in measuring the radon activity concentration in dwellings, where the results were successfully compared with two commercially available measurement methods. The application of PADC detectors in the detection of heavy charged particles could be based on simulations in the SRIM program in future research.

In addition to ongoing cooperation focused on the use of artificial intelligence, the recent research at STU is currently focused on changes in the response of PADC detectors due to exposure to high doses of gamma radiation. Individual topics for future research can be developed independently within the framework of projects and final theses.

Závěr

Cílem dizertační práce bylo vyvinout metodiku pro použití SSNTD detektorů typu PADC a implementovat navrhovaná opatření do měření dozimetrických veličin. Bylo definováno pět témat disertační práce, zaměřených na různé aspekty použití PADC detektorů. Tento text představil stručný přehled fungování SSNTD detektorů a metod jejich zpracování, včetně softwarových nástrojů vyvinutých autorkou dizertační práce. Většina experimentů provedených v rámci dizertační práce byla publikována. V době odevzdání dizertační práce byly čtyři články v recenzním řízení.

V rámci dizertační práce bylo provedeno několik experimentů s různými zdroji ionizujícího záření, jako jsou radioizotopové neutronové zdroje Am-Be a Pu-Be, ale také jiné neutronové zdroje, jako jsou D-D, nebo různé kanály experimentálního reaktoru TRIGA Mark-II. Detektory byly také ozářeny ^{252}Cf , ^{241}Am a byly také použity k měření objemové aktivity radonu v obytných prostorách. Na základě simulací bylo navrženo použití radiátorů HDPE a Kapton, které bylo následně ověřeno experimentálně. Byl navržen hliníkový degradér, ale jeho použití při experimentu nebylo nutné.

Leptací postupy na STU vycházejí z doporučení společnosti Tasl a byly upravovány podle účelu experimentu. Účast ve skupině EURADOS umožňuje STU jako členovi porovnávat data s laboratořemi, které používají jiné leptací postupy. Byla ověřena změna odezvy při změně doby leptání a byla navržena odpovídající korekce.

Pokud jde o vnější podmínky, byla stanovena metodika pro zacházení s detektory po celou dobu jejich životnosti, ať už z hlediska přepravy, manipulace nebo skladování (při zohlednění prováděných experimentů).

Kód Neutron_CR-39 byl opraven a uzpůsoben tak, aby jeho nastavení odpovídalo reálným experimentálním podmínkám na STU, včetně limitů pro velikost leptaných stop. Kód byl také upraven tak, aby bylo možné jej spustit s vstupními daty získanými z MCNP. To umožnilo simulace, jako je energetická závislost odezvy detektorů PADC.

V průběhu doktorského studia bylo provedeno několik experimentů, na jejichž základě byla sestavena metodika práce s detektory PADC pro různé aplikace. Bylo vyvinuto několik softwarových nástrojů, které umožňují zpracování naměřených dat.

V rámci disertační práce byly také identifikovány oblasti potenciálního budoucího výzkumu. Jedním z možných směrů výzkumu je pokračování spolupráce s týmy odborníků v oblasti umělé inteligence a strojového učení, kteří v současné době pracují s daty z minulých experimentů v rámci projektu PANDORA. Tato spolupráce by mohla vést k přesnějšímu rozpoznávání leptaných stop a tím ke snížení nejistoty měření. Pokračování ve vývoji analýzy detektorů PADC na základě PCA a klastrovacích mechanismů, jak bylo v dizertační práci navrženo, úzce souvisí s předchozí oblastí. Tato kombinace by mohla být vhodná například pro použití detektorů PADC v jaderných forenzních metodách. Dalším směrem je neutronová radiografie, pro kterou byly stanoveny počáteční podmínky a byla provedena první demonstrační ukáзка. Použití detektorů PADC v disertační práci se osvědčilo také při měření objemové aktivity radonu v obytných prostorách, kde byly výsledky úspěšně porovnány se dvěma komerčně dostupnými měřicími metodami. Aplikace detektorů PADC při detekci těžkých nabitých částic by mohla být v budoucím výzkumu založena na simulacích v programu SRIM.

Kromě pokračující spolupráce zaměřené na využití umělé inteligence se současný výzkum na STU zaměřuje na změny v odezvě detektorů PADC v důsledku vystavení vysokým dávkám gama záření. Jednotlivá témata pro budoucí výzkum mohou být rozvíjena samostatně v rámci projektů a závěrečných prací.

References

- [1] PAUL, Sabyasachi, S.P. TRIPATHY, G.S. SAHOO, T. BANDYOPADHYAY, and P.K. SARKAR. Measurement of fast neutron spectrum using CR-39 detectors and a new image analysis program (autoTRAK_n). *Nuclear Instruments and Methods in Physics Research Section A: Accelerators, Spectrometers, Detectors and Associated Equipment* [online]. Elsevier BV, 2013, 729, 444-450 [cited 2025-10-20]. ISSN 0168-9002. Available from: doi:10.1016/j.nima.2013.07.083
- [2] JAMES F. ZIEGLER, Matthias ZIEGLER, and J.P BIRSACK. SRIM – The stopping and range of ions in matter (2010). *Nuclear Instruments and Methods in Physics Research Section B Beam Interactions with Materials and Atoms* [online]. 2010, 2010-02-27, **268**(11-12), 1818-1823 [cited 2025-10-20]. ISSN 0168-583X. Available from: doi:10.1016/j.nimb.2010.02.091
- [3] BOLZONELLA, M., I. AMBROŽOVÁ, M. CARESANA, et al. Neutron personal dosimetry using polyallyl diglycol carbonate (PADC): Current status, best practices and proposed research. *Physics Open* [online]. Elsevier BV, 2022, **12**, 100114 [cited 2025-10-20]. ISSN 2666-0326. Available from: doi:10.1016/j.physo.2022.100114
- [4] AMIT, Gal, Idan MOSSERI, Ofir EVEN-HEN, et al. Particles Detection System with CR-39 Based on Deep Learning. *Laser and Particle Beams* [online]. Cambridge University Press (CUP), 2022, 2022-6-29, **2022** [cited 2025-10-20]. ISSN 0263-0346. Available from: doi:10.1155/2022/3820671
- [5] KADHIM, Nada Farhan, Yasser Ayad KADHIM, Rasha S. AHMED, Ali A. RIDHA, and Mostafa Y. A. MOSTAFA. The impact on alpha emission rates of varying distances between a CR-39 detector and alpha-emitting bone samples. *Radiation Detection Technology and Methods* [online]. Springer Science and Business Media, 2021, 2021-11-16, **5**(4), 618-626 [cited 2025-10-20]. ISSN 2509-9930. Available from: doi:10.1007/s41605-021-00291-4
- [6] SHABAAN, Doaa H., Entesar H. EL-ARABY, R. YAJZEY, Amel AZAZI, and Sahr ALZHRANI. Evaluation of the radiation emission of radon gas from various building materials. *Journal of Radiation Research and Applied Sciences* [online]. Elsevier BV, 2025, 18(1), 101194 [cited 2025-10-21]. ISSN 1687-8507. Available from: doi:10.1016/j.jrras.2024.101194
- [7] SHOEIB, M.Y., Morsy A. EL-APASERY, Doaa A. AHMED, and A.F. ABD-ELRAHEEM. Determination of Radium concentration and Radon Exhalation Rates Using CR-39 Detector for Different Geopolymer Cement Samples Containing Industrial Wastes. *Radiation Physics and Chemistry* [online]. Elsevier BV, 2024, **222**, 111790 [cited 2025-10-21]. ISSN 0969-806X. Available from: doi:10.1016/j.radphyschem.2024.111790
- [8] EL-ARABY, Entesar H. and Doaa H. SHABAAN. Measurement of radioactive concentration in different foodstuffs consumed in Jazan region. *Food Chemistry* [online]. Elsevier BV, 2023, **424**, 136363 [cited 2025-10-21]. ISSN 0308-8146. Available from: doi:10.1016/j.foodchem.2023.136363
- [9] TRACK ANALYSIS SYSTEMS LTD [TASL]. *Track Analysis Systems Ltd* [online]. [cited 2023-11-29]. Available from: <https://www.tasl.co.uk/>
- [10] FROMM, Michel, Satoshi KODAIRA, Tamon KUSUMOTO, Rémi BARILLON, and Tomoya YAMAUCHI. Role of intermediate species in the formation of ion tracks in PADC: A review. *Polymer Degradation and Stability* [online]. Elsevier BV, 2019, **161**, 213-224 [cited 2025-11-18]. ISSN 0141-3910. Available from: doi:10.1016/j.polymdegradstab.2019.01.028
- [11] DURRANI, S. A. and R. K. BULL. *Solid State Nuclear Track: Principles, Methods and Applications*. Oxford: Pergamon Press, 1987. International Series in Natural Philosop. vol. 111. ISBN 978-0-08-020605-9.

- [12] MOHAMMAD REZA DEEBAND, Parviz ABDOLMALEKI, MOHAMMAD REZA KARDAN, Hossein KHOSRAVI, and M. TAHERI. An investigation on the response of PADC detectors to neutrons. *Applied Radiation and Isotopes* [online]. 2010, 2010-10-21, **69**(2), 340-345 [cited 2025-11-19]. ISSN 0969-8043. Available from: doi:10.1016/j.apradiso.2010.10.009
- [13] M.A. STANOJEV PEREIRA, J.G. MARQUES, R. PUGLIESI, and J. P. SANTOS. Improved track-etch neutron radiography using CR-39. *Nuclear Instruments and Methods in Physics Research Section A Accelerators Spectrometers Detectors and Associated Equipment* [online]. 2014, 2014-08-07, **764**, 310-316 [cited 2025-11-19]. ISSN 0168-9002. Available from: doi:10.1016/j.nima.2014.07.061
- [14] CARESANA, M., M. FERRARINI, Alessandro PORTA, and Fabrizio CAMPI. Performance evaluation of a radiator degrader CR39 based neutron spectrometer. *Nuclear Instruments and Methods in Physics Research Section A Accelerators Spectrometers Detectors and Associated Equipment* [online]. 2012, 2012-04-12, **680**, 155-160 [cited 2025-11-19]. ISSN 0168-9002. Available from: doi:10.1016/j.nima.2012.02.050
- [15] BOLZONELLA, M., I. AMBROŽOVÁ, M. CARESANA, et al. Neutron personal dosimetry using polyallyl diglycol carbonate (PADC): Current status, best practices and proposed research. *Physics Open* [online]. 2022, **12** [cited 2025-05-06]. ISSN 26660326. Available from: doi:10.1016/j.physo.2022.100114
- [16] FILOVÁ, Vendula, Branislav VRBAN, Pavol BLAHUŠIAK, Jakub LÜLEY, Štefan ČERBA, and Vladimír NEČAS. The acceptance testing of PADC detectors for fast neutron dosimetry using PuBe neutron source. *Radiation Physics and Chemistry* [online]. 2023, **212** [cited 2024-01-22]. ISSN 0969806X. Available from: doi:10.1016/j.radphyschem.2023.111181
- [17] HERMSDORF, D. Measurement and comparative evaluation of the sensitivity V for protons and hydrogen isotopes registration in PADC detectors of type CR-39. *Radiation Measurements* [online]. 2009, 2009-10-01, **44**(9-10), 806-812 [cited 2025-11-19]. ISSN 1350-4487. Available from: doi:10.1016/j.radmeas.2009.10.084
- [18] NIKEZIĆ, D. and K.N YU. Computer program TRACK_TEST for calculating parameters and plotting profiles for etch pits in nuclear track materials. *Computer Physics Communications* [online]. 2005, 2005-11-16, **174**(2), 160-165 [cited 2025-11-19]. ISSN 0010-4655. Available from: doi:10.1016/j.cpc.2005.09.011
- [19] NIKEZIĆ, D., Miloš IVANOVIĆ, and K.N YU. A computer program TRACK_P for studying proton tracks in PADC detectors. *SoftwareX* [online]. 2016, 2016-01-01, **5**, 74-79 [cited 2025-11-19]. ISSN 2352-7110. Available from: doi:10.1016/j.softx.2016.04.006
- [20] MILENKOVIĆ, Biljana, N. STEVANOVIĆ, D. NIKEZIĆ, and Miloš IVANOVIĆ. Computer program Neutron_CR-39 for simulation of neutrons from an Am–Be source and calculation of proton track profiles. *Computer Physics Communications* [online]. 2011, 2011-04-15, **182**(7), 1536-1542 [cited 2025-11-19]. ISSN 0010-4655. Available from: doi:10.1016/j.cpc.2011.03.024
- [21] WERNER, C. J., J. S. BULL, M. J. GROSSKOPF, J. S. HENDRICKS, H. G. HUGHES, R. C. JOHNS, D. B. PELOWITZ, R. E. PRAEL, J. E. SWEEZY, L. S. WATERS et al. *MCNP6.2 User's Manual* [online]. Los Alamos: Los Alamos National Laboratory, 2018, LA-UR-17-29981, Rev. 1. Available from: <https://mcnp.lanl.gov/pdf_files/LA-UR-17-29981.pdf>. [cited 3 April 2025].
- [22] VRTALOVÁ, Vendula, Branislav VRBAN, Jakub LÜLEY, Štefan ČERBA, Matúš SEDLÁK, Filip RÉVAI, Otto GLAVO, and Vladimír NEČAS. *Neutron field spatial distribution from the DD neutron source determined by the KOSTKA experimental device*. Article under review, 2025.

- [23] NIKEZIĆ, D. and K.N YU. Formation and growth of tracks in nuclear track materials. *Materials Science and Engineering R Reports* [online]. 2004, 2004-09-21, **46**(3-5), 51-123 [cited 2025-11-25]. ISSN 0927-796X. Available from: doi:10.1016/j.mser.2004.07.003
- [24] F. B. MALIK, E.U KHAN, I.E QURESHI, S. N. HUSAINI, M. SAJID, Shafqat KARIM, and Khalid JAMIL. Swelling in CR-39 and its effect on bulk etch-rate. *Radiation Measurements* [online]. 2002, 2002-08-01, **35**(4), 301-305 [cited 2025-11-19]. ISSN 1350-4487. Available from: doi:10.1016/s1350-4487(02)00053-7
- [25] FILOVÁ, Vendula, VRBAN, Branislav, ČERBA, Štefan, LÜLEY, Jakub, GLAVO, Otto, and NEČAS, Vladimír. *Software for analysis of ionizing radiation measurement data from PADC track detectors*. In: KOZÁKOVÁ, Alena (ed.). *ELITECH'24: 26th Conference of Doctoral Students*. Bratislava: Vydavateľstvo Spektrum STU, 2023. ISBN 978-80-227-5409-5.
- [26] *A Comprehensive Framework enabling the Delivery of Trustworthy Datasets for Efficient AIoT Operation* [online]. 2024, 2024-04-01 [cited 2025-10-20]. Available from: doi:10.3030/101135775
- [27] STABILINI, Alberto, M.S AKSELROD, Vasilij FOMENKO, Jonathan HARRISON, and E.G YUKIHARA. Principal Component Analysis applied to neutron dosimetry based on PADC detectors and FNTDs. *Radiation Measurements* [online]. 2021, 2021-01-29, **141**, 106516-106516 [cited 2025-11-19]. ISSN 1350-4487. Available from: doi:10.1016/j.radmeas.2021.106516
- [28] VRTALOVÁ, Vendula, Branislav VRBAN, Štefan ČERBA, Jakub LÜLEY, Otto GLAVO, and Filip RÉVAI. *Angular Dependence of PADC Detectors Response in Alpha Radiation Measurements*. Article submitted to journal, 2025.
- [29] FILOVÁ, Vendula, VRBAN, Branislav, BLAHUŠIAK, Pavol, ČERBA, Štefan, LÜLEY, Jakub, GIBALA, Samuel, GLAVO, Otto, RÉVAI, Filip and NEČAS, Vladimír. Performance of PCA in PADC Detector Analysis for Fast Neutron Measurement. Accepted for publication, 2025.
- [30] VRTALOVÁ, Vendula, Branislav VRBAN, Pavol BLAHUŠIAK, Jakub LÜLEY, Štefan ČERBA, Filip RÉVAI, Otto GLAVO. *Etching Time Effects on Fast Neutron Response in PADC Detectors*. Article submitted to journal, 2025.
- [31] FILOVÁ, Vendula, Branislav VRBAN, Pavol BLAHUŠIAK, Štefan ČERBA, Jakub LÜLEY, Otto GLAVO, and Vladimír NEČAS. Coupling of a PADC detector and a PE radiator for neutron radiography. *AIP conference proceedings* [online]. 2024, 2024-01-01, **3251**, 070004-070004 [cited 2025-11-25]. ISSN 0094-243X. Available from: doi:10.1063/5.0234120
- [32] VRTALOVÁ, Vendula, Branislav VRBAN, Pavol BLAHUŠIAK, Štefan ČERBA, Jakub LÜLEY, Otto GLAVO, Filip RÉVAI, Vladimír NEČAS. *The Study of Fading of the PADC Detectors Irradiated by Fast Neutrons*. Article submitted to journal, 2025.
- [33] FILOVÁ, Vendula, Branislav VRBAN, Pavol BLAHUŠIAK, Štefan ČERBA, Jakub LÜLEY, Otto GLAVO, and Vladimír NEČAS. Initial approaches for establishing fast neutron radiography with PADC material. *European Physical Journal Special Topics* [online]. 2025, 2025-02-03 [cited 2025-11-25]. ISSN 1951-6355. Available from: doi:10.1140/epjs/s11734-025-01481-7
- [34] M.A. STANOJEV PEREIRA, J.G MARQUES, R. PUGLIESI, and J. P. SANTOS. Improved track-etch neutron radiography using CR-39. *Nuclear Instruments and Methods in Physics Research Section A Accelerators Spectrometers Detectors and Associated Equipment* [online]. 2014, 2014-08-07, **764**, 310-316 [cited 2025-11-19]. ISSN 0168-9002. Available from: doi:10.1016/j.nima.2014.07.061
- [35] VRTALOVÁ, Vendula, Branislav VRBAN, Jakub LÜLEY, Štefan ČERBA, M. SEDLÁK, Filip RÉVAI, Otto GLAVO, and Vladimír NEČAS. Neutron field spatial distribution from the DD neutron source determined by the KOSTKA experimental device. *EPJ Web of Conferences* [online]. 2025, 2025-01-

01, **338**, 10015-10015 [cited 2025-11-25]. ISSN 2100-014X. Available from: doi:10.1051/epjconf/202533810015

- [36] GRÜEBLER, W., W. D. M. RAE, and M. W. McNAUGHTON. DROSG-2000: A Computer Program for Calculating Neutron Spectra from 2-Body Reactions. Vienna: IAEA Nuclear Data Section, 2000. IAEA-NDS-87, Rev. 9 [online]. [cited 2025-11-25]. Available from: <https://www-nds.iaea.org/drosg2000.html>

Publications of the author related to the thesis

V2 Scientific outcome of publishing activities as part of an edited book or proceedings

- V2_01 **FILOVÁ, Vendula**; VRBAN, Branislav; BLAHUŠIAK, Pavol; ČERBA, Štefan; LÜLEY, Jakub; GIBALA, Samuel, GLAVO, Otto; RÉVAI, Filip and NEČAS, Vladimír. Performance of PCA in PADC Detector Analysis for Fast Neutron Measurement. In: Jozef, SITEK; Ján, VAJDA and Igor, JAMNICKÝ. APCOM 2025. Melville: AIP Publishing. Accepted for publication.
- V2_02 **VRTALOVÁ, Vendula**; VRBAN, Branislav; LÜLEY, Jakub; ČERBA, Štefan; SEDLÁK, Matúš; RÉVAI, Filip; GLAVO, Otto and NEČAS, Vladimír. Neutron field spatial distribution from the DD neutron source determined by the KOSTKA experimental device. EPJ Web Conf. ANIMMA 2025 – Advancements in Nuclear Instrumentation Measurement Methods and their Applications, 338. p. 10015. 2025.
- V2_03 **FILOVÁ, Vendula**; VRBAN, Branislav; BLAHUŠIAK, Pavol; ČERBA, Štefan; LÜLEY, Jakub and NEČAS, Vladimír. Performance of PADC Track Detectors in Fast Neutron Dosimetry Under Different Etching Conditions. In: Jozef, SITEK; Ján, VAJDA and Igor, JAMNICKÝ. APCOM 2023. Melville: AIP Publishing, 2024, ISBN 978-0-7354-4805-6.
- V2_04 KORNHAUSER, Matúš; ČERBA, Štefan; **FILOVÁ, Vendula**; VRBAN, Branislav; LÜLEY, Jakub, and NEČAS, Vladimír. Deterministic Evaluation of Digital Images of Passive Radiation Detectors. In: Jozef, SITEK; Ján, VAJDA and Igor, JAMNICKÝ. APCOM 2023. Melville: AIP Publishing, 2024, ISBN 978-0-7354-4805-6.
- V2_05 **FILOVÁ, Vendula**; VRBAN, Branislav; BLAHUŠIAK, Pavol; ČERBA, Štefan; LÜLEY, Jakub; GLAVO, Otto and NEČAS, Vladimír. Coupling of a PADC Detector and a PE Radiator for Neutron Radiography. In: Jozef, SITEK; Ján, VAJDA and Igor, JAMNICKÝ. APCOM 2024. Melville: AIP Publishing, 2024,
- V2_06 **FILOVÁ, Vendula**; VRBAN, Branislav; ČERBA, Štefan; LÜLEY, Jakub; NEČAS, Vladimír and DUGDALE, Maria. Performance testing of the system for analysis of PADC track detectors for neutron dosimetry. In: Jozef, SITEK; Ján, VAJDA and Igor, JAMNICKÝ. APCOM 2022. Melville: AIP Publishing, 2023, ISBN 978-0-7354-4479-9.
- V2_07 KORNHAUSER, Matúš; ČERBA, Štefan and **FILOVÁ, Vendula**. Deterministic evaluation of digital images from passive radiation detectors. In: Peter, BENKO and Stanislav, SOJAK. ŠVOČ 2023. Bratislava: Vydavateľstvo Spektrum STU, 2023, pp. 170-173. ISBN 978-80-227-5307-4.

O2 Technical outcome of publishing activity as part of an edited book or proceedings

- O2_01 **FILOVÁ, Vendula**. Directional response of PADC detectors in alpha radiation measurement. In: Matěj, RZEHULKA. Nuclear energy in the work of the younger generation - 2023. Prague: Czech Nuclear Society, 2024, p. 79. ISBN 978-80-02-03050-8.
- O2_02 **FILOVÁ, Vendula**; VRBAN, Branislav; ČERBA, Štefan; LÜLEY, Jakub; and NEČAS, Vladimír. Software for analysis of ionizing radiation measurement data from PADC track detectors. In: Alena, KOZÁKOVÁ. ELITECH'24. Bratislava: Vydavateľstvo Spektrum STU, 2024, ISBN 978-80-227-5409-5.

- O2_03 **FILOVÁ, Vendula**; VRBAN, Branislav; BLAHUŠIAK, Pavol; LÜLEY, Jakub; ČERBA, Štefan and NEČAS, Vladimír. Problematics of handling PADC detectors of the TASTRAK type in fast neutron dosimetry. In: Alena, KOZÁKOVÁ. ELITECH'23. Bratislava: Vydavateľstvo Spektrum STU, 2023, ISBN 978-80-227-5298-5.
- O2_04 **FILOVÁ, Vendula**; VRBAN, Branislav; ČERBA, Štefan; LÜLEY, Jakub, and NEČAS, Vladimír. Experimental study of etching condition effects and alpha radiation on TASTRACK PADC detectors. In: Silvia, DULANSKÁ; Iveta, SMETANOVÁ and Ján, KUBANČÁK. XLIII. Radiation Protection Days 2022: Book of Abstracts. Stará Lesná, Slovak Republic. November 19–23, 2022. 1st ed. Bratislava: Slovak Medical University, 2022, p. 40. ISBN 978-80-89702-98-5.
- O2_05 VRBAN, Branislav; LÜLEY, Jakub; **FILOVÁ, Vendula**; BLAHUŠIAK, Pavol; ČERBA, Štefan; BONKOVÁ, Ivana and NEČAS, Vladimír. Calibration of radon dosimetry system with radon chamber in self-decay mode. In: Silvia, DULANSKÁ; Iveta, SMETANOVÁ and Ján, KUBANČÁK. XLIII. Radiation Protection Days 2022: Book of Abstracts. Stará Lesná, Slovak Republic. November 19–23, 2022. 1st ed. Bratislava: Slovak Medical University, 2022, p. 50. ISBN 978-80-89702-98-5.

V3 Scientific outcome of publication activity from the journal

- V3_01 **FILOVÁ, Vendula**; VRBAN, Branislav; BLAHUŠIAK, Pavol; ČERBA, Štefan; LÜLEY, Jakub; GLAVO, Otto; NEČAS, Vladimír. Initial approaches for establishing of the fast neutron radiography with PADC material. The European Physical Journal Special Topics. 2025.
- V3_02 **FILOVÁ, Vendula**; LESAY, Vladimír; HOLEČEK, Josef; VRBAN, Branislav; LÜLEY, Jakub; ČERBA, Štefan; GLAVO, Otto; NEČAS, Vladimír. Interlaboratory comparison of methods for determining radon activity concentration in dwellings in Slovakia and the Czech Republic. Radiation Physics and Chemistry, 229. p. 112429. 2025.
- V3_03 **FILOVÁ, Vendula**; VRBAN, Branislav; BLAHUŠIAK, Pavol; LÜLEY, Jakub; ČERBA, Štefan; NEČAS, Vladimír. The acceptance testing of PADC detectors for fast neutron dosimetry using PuBe neutron source. Radiation Physics and Chemistry, 212. p. 111181. 2023.
- V3_04 LÜLEY, Jakub; **FILOVÁ, Vendula**; BLAHUŠIAK, Pavol; VRBAN, Branislav; ČERBA, Štefan; BONKOVÁ, Ivana; NEČAS, Vladimír. CR-39 detector-based Radon dosimetry system calibration in the self-decay mode. European Physical Journal - Special Topics, 232. p. 1493-1500. 2023.

Citations of the publications of the author of the thesis

V3_03 **FILOVÁ, Vendula**; VRBAN, Branislav; BLAHUŠIAK, Pavol; LÜLEY, Jakub; ČERBA, Štefan; NEČAS, Vladimír. The acceptance testing of PADC detectors for fast neutron dosimetry using PuBe neutron source. *Radiation Physics and Chemistry*, 212. p. 111181. 2023.

Citations:

[1] SAHOO, G.S.; PAUL, S.; TRIPATHY, S.P.; CHAUDHARY, N. and SRINIVASAN, P. An approach to measure low LET radiation at high dose using CR-39 track detector. *Applied Radiation and Isotopes*, 221. p. 111817. 2025.

V3_04 LÜLEY, Jakub; **FILOVÁ, Vendula**; BLAHUŠIAK, Pavol; VRBAN, Branislav; ČERBA, Štefan; BONKOVÁ, Ivana; NEČAS, Vladimír. CR-39 detector-based Radon dosimetry system calibration in the self-decay mode. *European Physical Journal - Special Topics*, 232. p. 1493-1500. 2023.

Citations:

[1] HU, Jun; KRANROD, Chutima; PRADANA, Radhia; MUSIKAWAN, Saowarak; OMORI, Yasutaka; HOSODA, Masahiro; KODAIRA, Satoshi; TOKONAMI, Shinji. Evaluation of stochastic method on track density analysis for passive radon measurement. *Applied Radiation and Isotopes*, 225. p. 111998. 2025.

[2] AHMED, R.S. The Effective Dose in Specific Organs and Excess Lifetime Cancer Risk Due to Soil ^{222}Rn in Iraq/Baghdad, with Simultaneous Analysis Of ^{214}Po , ^{218}Po , ^{226}Ra , And ^{238}U Activity Concentrations. *Soil and Sediment Contamination: An International Journal*, p. 1—17. 2025

[3] BABAK, Vitalii; BABAK, Serhii; EREMENKO, Volodymyr; KUTS, Yurii a ZAPOROZHETS, Artur. Transducers of Information-Measuring Systems. In: *Studies in systems, decision and control*. p. 249-306. 2025. ISSN 2198-4182.

[4] HU, Jun; KRANROD, Chutima; OMORI, Yasutaka; HOSODA, Masahiro; TOKONAMI, Shinji. Radiation dose estimation for indoor radon, thoron and their progenies using a stochastic method—a small-scale survey in Wuhan, China. *Radiation Protection Dosimetry*, 200. p. 1720-1725. 2024.